DECAY OF WEAK TURBULENCE

by

S.C. Ling and T.T. Huang

June 1969

Department of Space Science and Applied Physics
The Catholic University of America
Washington, D.C. 20017

ABSTRACT

A detailed experimental investigation of the structure of weak turbulence generated by various single-and multiple-stage grids has been made. The weak turbulent fields were limited to those having no interaction with the mean flow field. The present study covers a range of Reynolds numbers of turbulence between 70 and 7. Components of turbulence were found to have equipartition of energy in the final stage of decay. When the Reynolds number of turbulence is < 30, the kinetic energy of turbulence decreases inversely as the square of decay time. All the length scales of turbulence increase as the square root of time, while the Reynolds number of turbulence decreases as the square root of time. Both the measured spectral and correlation functions showed self-preserving forms that were not in agreement with those predicted by the normal statistics of turbulence. The longitudinal correlation function is closer to a Cauchy's distribution than a Gaussian distribution function. The resultant three-dimensional energy spectrum show continuous transfer of energy from the low to high wave numbers through out the final stage of decay. The measured time-correlation functions up to the fourth order indicate that the grid-generated turbulence is not completely consistent with normal statistics. All experimental evidences imply that in the final stage of decay the wave components of turbulence are not completely independent with unlimited degrees of freedom but are closely related to the kinetic model of a field consisting of a specific type of line vortices which are aged and essentially non-interacting.

i

CONTENTS

LIST OF FIGURES

1.0 INTRODUCTION

In almost forty years of research in turbulence, the classical problem of how a weak turbulent field decays with time is still an unsettled question. The traditional statistical treatment of turbulence is to derive from the Navier-Stokes equations the correlation equations for fluctuating velocities at two and three points in the flow field. The second-order correlation equations contain the third-order correlations. Equations for the third-order correlations can be obtained, but these involve the fourth-order correlations, and so on. In a weak turbulent field, i.e., in a final period of decay, the third-order correlations are usually assumed negligible, and then the second-order correlations become linear differential equations. The energy spectrum tensor of the turbulent velocity fluctuations, which are Fourier transformations of the second-order correlations, are introduced to provide the basis for ideas about the energy distribution among different wave numbers. Solutions of the energy spectrum tensor for the weak turbulent field can be expressed by the product of an exponential time-decay function with an unspecified initial spectrum tensor. Early theoretical investigations of this subject were made by Taylor[1], Millionshtchikov[2], Kármán-Howarth[3], Loitsiansky[4], and Lin[5]. Upon assuming the Loitsiansky invariant, Batchelor[6] found that the energy of a homogeneous and isotropic turbulence decays as $(t-t_0)^{-5/2}$ in the final period, where t is the time, and t_0 is a virtual time. The Loitsiansky invariant was used to postulate the unspecified initial spectrum tensor. Retaining the hypothesis of homogeneity, Batchelor and Chandrasekhar[7] extended the analysis for anisotropic turbulence. They again arrived at the same

power law to the -5/2 for the final period of energy decay. Inhomogeneous turbulence was further analyzed by Deissler[8]. When the energy spectrum tensor near the origin of wave-number space is taken to be the same as that assumed by Batchelor for homogeneous turbulence, all components of wave energy are found to decay as the power law to -5/2.

However, Philips[9] and recently Saffman[10] found that the energy in the final period decays as $(t-t_0)^{-3/2}$, if the net linear momentum of the fluid is not zero. Birkhoff[11] pointed out that a decay law between -3/2 and -5/2 power in the final period had theoretical possibility compatible with the Navier-Stokes and the continuity equations. Recently Lee and Tan[12], indicated that the initial spectrum tensors, which ultimately led to decay laws to the -5/2 and -2 powers in the final period of an innomogeneous turbulence, were a class of admissible tensors satisfying the conservation of mass and the symmetrical condition of the spectrum tensor.

Although the statistical theory for the weak turbulent field attracted so much attention, only a few experimental investigations appear in the literature. Validity of the statistical theory for turbulence in the final period has not been verified in detail. The experimental evidence made by Batchelor and Townsend[13] to confirm the energy decay law of the -5/2 power was considered by Birkhoff[11] to be inconclusive. Further experimental study on weak decaying turbulence seems to be necessary to clarify the analytical predictions. The experimental result of Tan and Ling[14] shows that the energy of turbulence decays as t^{-2} within a substantial

range of final decay time. A kinetic model, based on aged and noninteracting

line vortices, was proposed to explain this observation; however, no spectrum

measurement was made at that time. Deissler[15] suggested that spectrum measurement

in the final period would be necessary for positive identification of the structure

of weak turbulence. Hence, under his encouragement and support, an intensive

restudy of the structure of a weak turbulent field was undertaken. An improved

testing facility was built with the specific objective of extending the decay time

as long as possible so as to obtain a more accurate indication of the decay law.

The specific turbulent field studied in this paper can be classified as one

of low Reynolds number of turbulence (<100) with physical eddies of limited range

in size and energy. Furthermore, these eddies do not have interaction with the

mean flow field. To generate such a flow field, several methods were considered.

1. Generation of turbulence by placing a grid in a uniform steady

    flow field,

2. Generation of turbulence by a grid moving at uniform speed through

    an initially quiescent body of fluid, and

3. Generation of uniform turbulence throughout the volume of an

    initially quiescent large body of fluid by dropping a grid quickly

    through the body of fluid.

The third method of generating turbulence is considered to be most ideal in that the

energy gradient of turbulence will be minimum throughout the volume of fluid.

However, it has the same common defect associated with the second method because

it is difficult to avoid small secondary fluid motions caused by nonuniform temperatures existing in a large body of stagnant fluid. Furthermore, if one employs the hot wire or hot film techniques to obtain statistical data for the turbulent field, one would be required to tow the sensor mechanically through the body of fluid at a high degree of uniform speed. This was found to be very difficult to achieve, considering the present state of the art as well as the need to maintain a reasonable cost. Most of all, the length of each statistical record that could be obtained from these methods is critically limited by the size of any testing facilities. The overall characteristic of the first method was found to be the best of all three in that uniform temperature could be maintained through the continuous recirculating and mixing processes employed in the system. Due to the great inertia of a flowing body of fluid, noise, vibration, and unsteady flow can be reduced to a desirable limit. In addition, the sensor can remain stationary with respect to the laboratory frame, thus eliminating an important source of noise. Above all, unlimited amounts of statistical data could be obtained in such a system. Therefore, this method was adopted to generate all turbulences studied in this report.

Detailed techniques for the experimental setup, measurements, data reductions, and analytical results are described in the following sections. In general, the turbulence in its final stage of decay was found to have a distinctive self-preserving velocity structure. The wave components of such a field do not show any tendency to decay independently, even at very low Reynolds number of turbulence. The measured energy transfer function indicates continuous transfer of energy from the low

to high wave numbers throughout the final stage of decay. This was found to be the

key experimental fact which is contrary to the present theory of weak turbulence,

in which the transfer of energy other than the self diffusion of waves is taken

to be zero in the limit. A maximum energy decay rate proportional to the inverse

square of decay time was consistently observed for a weak turbulent field that

did not interact with the mean flow field. For turbulence which interacts with the

mean flow field, the decay rate is always less than the inverse-square law. All

attempts to create turbulent fields that would decay faster than the inverse-square

law as well as the predicted -5/2 power law have not been successful. It is now

doubtful whether such a field could be created or exist within the physical limits

of interest.

2.0 EXPERIMENTAL SETUP AND PROCEDURE

2.1 Water Channel

A water channel instead of a wind tunnel was selected for the present study because the kinematic viscosity of water is approximately 16 times less than that of air. Hence, for modeling a given Reynolds number, either based on the mesh length of the turbulence generating grid or the dissipation length of the grid generated turbulence, the mean velocity required for water is only one-sixteenth that of air. Also there will be a corresponding increase in time scale for water as against air. The required Reynolds numbers, based on the mesh length and the dissipation length, are of the order of <1000 and <100, respectively, for the present study. The 16 times reduction in mean velocity for water would not only keep the boundary layer of the channel laminar to reduce the interaction with the turbulent field, but also the corresponding increase in the time scale would enhance the accuracy of measurements for the decay rate of turbulence. The lengthened time scale also permits one to obtain a direct visual observation of the sturcture of turbulence using the dye-streak technique.

A special water channel 0.6 meter in width by 0.6 meter in depth and 11.0 meters in length was constructed of double layers of 1.9-cm marine plywood, as shown in Fig. 1. The walls of the channel were built to within 0.16 cm of the true straight line by carefully overlapping the joints of the plywood panels. For a designed flow speed of less than 5 cm/sec, no measurable slope was necessary for the

bottom of the channel. The channel bottom was built to within 0.16 cm of the true level. The inside surface of the channel was lined with marine fiber-glass plastic and a smooth overcoat of paint. Two plastic pipes 10.2 cm in I.D. were used for recirculating the flow from one end of the channel to the other. At the outlet end of the channel, a 26.7-cm diameter low-velocity propeller pump was used for recirculating the fluid. The pump was driven by a special motor-generator set made by Electro-Craft Corporation. By means of feedback control, the motor speed was regulated against the output signal from the generator. A regulation within 0.02 percent of the set speed for all external variation of line voltages and changes in load was achieved.

Because of low speed of flow, no inlet contraction was needed to obtain uniform flow in the test section. Uniform flow in the channel was accomplished by using multiple sections of honeycomb and fine mesh screens. Since head loss through the screen was negligible, multiple layers of 12.6-mesh/cm screens were used to damp out all physical eddies larger than 0.1 cm. Small eddies of low energy level decayed very quickly within 10 cm from the last screen. To prevent clotting of the fine screens, water in the channel was filtered continuously by a swimming pool filter system to keep the water free of lint and bacterial growth. Conditions for uniform and steady flow in the channel were found to depend critically on the absolute uniformity of the damping screens; hence they were carefully cleaned at the beginning of each experiment. A baffle plate was installed at the outlet end of the channel. It was set at such a level that the water flowing over it would reach

the critical velocity shown in Fig. 1. Under this condition no waves downstream of the plate could propagate upstream; most of all, the backwater effect causing nonuniform flow in the channel was eliminated. The zone of stagnant flow field in front of the baffle plate was found to be less than half the width of the channel and it did not notably shorten the usable length of the test channel. Additional wave traps were installed at the inlet end to eliminate surface waves. To reduce external noises, the channel was set on a solid concrete floor far away from all sources of vibrations.

The low ambient noise of the test channel had been demonstrated by the fact that capillary dye streaks initiated at the inlet end of the channel remained straight to the outflow end. Dye drops introduced over the inlet wall surfaces diffused laminarly to approximately 2.0 cm from the wall at the outflow end. This indicated that the channel boundary layers were laminar throughout the channel when no turbulence-generating grid was introduced into the channel. With the introduction of turbulence generating grid used in this report, the dye drops introduced at the channel boundary near the grid were found to diffuse laterally about 5 cm from the wall 1 meter downstream from the grid. This was due mainly to the turbulence created by the grid. At the downstream end of the channel the lateral diffusion was limited to 8 cm because the boundary layer tended to remain laminar, and the grid turbulence decayed. Thus, the major protion of the channel core was free from either the disturbance generated from the channel walls or from the cutoff effect by the walls on the grid turbulence. These features were key reasons for using a water channel in preference to the wind tunnel for this study.

2.2 Biplane Grids

The mesh size of the turbulence-generating grid to be used was limited by the finite size of the water channel. The physical size of the turbulent eddies created by the grid should be small with respect to the width of the channel in order to avoid interaction of such eddies with the mean flow field. However, the mesh size should not be too small. The grid should be of a size that will produce turbulence of sufficient Reynolds number and energy that could still be detected at the outflow end of the channel. Three sizes of biplane square grids meeting the previously described requirements were used in this study. Two grids have the same mesh-to-rod ratio of $M/d = 2.8$, one with $M = 3.56$ cm and the other with $M = 1.78$ cm. The third is an open-type grid with $M/d = 5.0$ and $M = 3.18$ cm. Henceforth, these grids will be designated as Grids A, B and C, respectively. A detailed survey of the intensity of turbulence and grid wake was made immediately behind each of the three grids. In general, the grid wake can be detected at a distance of $x/M = 5$ behind the grid. Beyond $x/M = 5$, the wake becomes unstable. Farther downstream the wake is undetectable, and the turbulence becomes homogeneous in a plane normal to the mean flow. Measurements were taken to check the planar homogeneity of the generated turbulence at $x \geq 35\,M$ from Grids A and B, and at $x \geq 10\,M$ from Grid C. It was found that the measured intensities of turbulence were constant within 2 percent in the cross-flow planes. The energy components of turbulence were measured by varying the angle between the hot film sensor and the mean flow direction; see Section 2.3. The ratio of the energy of

turbulence in the flow direction, u^2, and the cross-flow direction, v^2, is shown in Fig. 2. The equipartition of the energy components of turbulence indicates that the turbulence in the present study has met a necessary condition of plane isotropy (within 5 percent). This result is different from the measurements of Batchelor and Stewart[16]. They reported the turbulence to be anisotropic ($u^2/v^2 = 1.5$) in the final period of decay after being apparently isotropic in the initial period.

2.3 Velocity Probe

Perfect low-frequency response and linear-output characteristics of a velocity probe are essential for measurement of weak turbulence in water. A linearized, constant-temperature hot-film anemometer system[17] was used to measure the fluctuating velocities. The basic sensor was a 30-degree, hot-film wedge, 0.15 mm in chord and 1.0 mm in span. The probe was mounted on brass tubing 2.5 mm in diameter by 10 cm in length. Both the velocity and the directional response of the probe were carefully calibrated; see Fig. 3. For the condition in which the fluctuating signal voltage e(t) and the turbulence velocity u(t) are linearly related, i.e., $e(t) = \beta u(t)$, the output signal from the sensor, whose plane of symmetry (bisecting plane of wedge) is parallel to the u and v component of the velocities, can be expressed by the following equation:

$$e(t) = \beta\{u(t)\cos\emptyset + v(t)\sin\emptyset\} + \Omega w(t) \qquad (2.1)$$

where ϕ is the angle between the mean velocity component U and the normal to

the long axis of the hot film; u(t) is the fluctuating velocity along U; v(t) and

w(t) are the cross velocity components normal to U; and ß and Ω are the

calibration constants. Both the constants ß and Ω and the directional sensitivity

were obtained and verified by oscillating the probe sinusoidally in a mean flow

field. The probe was oscillated mechanically in three different modes at a fixed

amplitude of 1.27 cm for different oscillating frequencies. In mode 1, the plane

of symmetry of the sensor was placed in the plane of u and v components, with

ϕ = 0 degree. The probe was oscillated along the direction of mean flow. In

mode 2, the film was set at ϕ = 45 degrees and was also oscillated along the

direction of the mean flow. In mode 3, the sensor was set back to ϕ = 0 degree

and was oscillated in the direction of the w component. Typical calibration

curves for the three modes are shown in Fig. 3. The slope of the calibration curve for

mode 1 gives the constant ß, while the slope of mode 3 gives the constant Ω . The

curve for mode 2 verifies the cosine response characteristics. The value of $\Omega/ß$

was found to be 0.09, which is negligible as far as the contribution of w^2 to the

measured quantities of u^2 and v^2 is concerned. When the plane of symmetry of the

probe is in the u and v plane, one notes that the relationship of e(t) and u(t)

is perfectly linear for both ϕ = 0 and 45 degrees throughout the range of measurement.

These ideal operating characteristics were built specifically into the anemometer

system for this work. The cosine direction sensitivity (Eq. 2.1) was found to break

down for ϕ > 55 degrees. Hence, Eq. 2.1 is valid for all turbulent fields studied,

except at locations very close to the grid where the instantaneous value of $\emptyset$ could exceed the previously described limit.

Let e_1 and e_2 be the root-mean-square (rms) outputs of the anemometer set at $\emptyset = 0$ degree and $\emptyset = 45$ degrees, respectively; then

$$\frac{\overline{u^2}}{\overline{v^2}} = \frac{e_1^2}{2e_2^2 - e_1^2} \tag{2.2}$$

This relationship was used to obtain the ratio of energy components shown in Fig. 2. Here we take $\overline{uv} = 0$, since there was no mean velocity gradient in the field.

2.4 Recording and Reprocessing Data

Signal output from the anemometer system was normally recorded on a frequency-modulated magnetic tape recorder. A continuous recording time of 35 minutes was used for each data run. Before a data run a calibration run was recorded by oscillating the probe at two frequencies ($f = 1/7$ and $1/14$ cps) in the mean flow field. The decaying turbulent fields were measured at approximately 10 locations along the channel, starting at a few mesh lengths from the grid and extending to a location where the energy of the ambient noise was approximately equal to 17 percent of the energy of turbulence. The ambient noise of the channel and equipment without the turbulence-generating grid was also recorded on the tape after each data run. During data recording, both the mean velocity and root-mean-square of turbulence were continuously monitored by analog means to provide assurance that the data were valid throughout the long recording period.

The recorded data can be analyzed either by an analog or by a digital computer. Most analog data-processing techniques use a low-pass RC filter to integrate the instantaneous quantities. Consequently, the resolution of the low-frequency result is not always too satisfactory. In analyzing data of a weak turbulence, especially in water, the low-frequency domain is extremely important since the bulk of energy is contained within the 2-cps region. To obtain unbiased measurements at low frequencies, digital computing techniques were chosen.

Before the recorded analog data could be analyzed by a digital computer the following reprocessing of data was required:

1. Transferral of the low-speed tape to a high-speed tape to meet the high speed capacity of the analog to digital converter.

2. Conversion of continuous analog data into discrete digital samples of equispaced time interval.

3. Removal of the long period trend and mean velocity U by means of a digital running-average technique.

The high-speed capability of the analog-to-digital converter required an increase in tape speed 32 times the original recording speed (4.78 cm/sec). This was done by speeding up the original tape recorded on an Ampex SP-300 by eight times and by transferring the data to a tape on an Ampex SR-600 recorder at a tape speed of 19 cm/sec. The transfer tape was then digitized at a speed four times faster than its recording speed.

To compute accurate autocorrelation and energy spectrum functions within

reasonable computer time, a careful trade-off study between the resolution of the results and the cost and capacity of the computer must be made. According to Blackman and Tukey[18], and Bendat and Piersol[19], a sample interval equal to one-fourth of the period of the highest frequency component observable in the record is sufficient for computing accurate autocorrelation and energy spectrum functions. From oscilloscope displays of the hot film output, the highest frequency component in the signal was about 10 cps. Thus, a sample interval of $\Delta t = 1/40$ second is used to digitize the analog data. It was found that the computed spectra contain almost no energy at frequencies higher than 5 cps; hence, the digitized sample interval used would not cause significant aliasing error.

The mean velocity and its long period trend may be removed from the original data, $e'(t)$, by a running average, $\overline{e_r'(t)}$.

$$e(t) = e'(t) - \overline{e_r'(t)} \tag{2.3}$$

where

$$\overline{e_r'(t)} = \frac{1}{2T} \int_{t-T}^{t+T} e'(\eta) \, d\eta$$

The effect of the running average on the recorded data can be seen as follows. The value of $e'(t)$ can be represented by a Fourier transform

$$e'(t) = \int_{-\infty}^{\infty} G'(f) \exp(i2\pi f t) \, df$$

and

$$G'(f) = \int_{-\infty}^{\infty} e'(t) \exp(-i2\pi f t) \, dt \tag{2.4}$$

The running average in terms of a Fourier transform can be obtained as

$$\overline{e_r'(t)} = \frac{1}{2T} \int_{t-T}^{t+T} \int_{-\infty}^{\infty} G'(f) \exp(i2\pi f\eta)\, d\eta\, dt$$

$$= \int_{-\infty}^{\infty} G'(f) \frac{\sin 2\pi fT}{2\pi fT} \exp(i2\pi ft)\, dt \tag{2.5}$$

It can be seen that the running average has a minimum high-frequency cutoff

effect proportional to $1/2\pi fT$ with band stops at $f = n/2T$, where $n = 1,2 \ldots$. It

follows that the Fourier transform of $e(t)$ is of the form

$$G(f) = G'(f) \left[1 - \frac{\sin 2\pi fT}{2\pi fT} \right] \tag{2.6}$$

and the power spectrum cutoff factor due to the running average is

$$\left[\frac{G(f) - G(f)}{G'(f)} \right]' = \left[\frac{\sin 2\pi fT}{2\pi fT} \right]' \tag{2.7}$$

For a low frequency of $f = 1/8T$, the power spectrum after removal of the running

average, $G(f)^2$, is equal to $0.005\, G'(f)^2$. On the other hand, if $f \geq 15/T$, then

we have a cutoff factor of less than 1 percent. A digital 5-minute running average

of $2T = 300$ seconds was used to remove both the mean velocity and the long period

trend from the original data. As can be seen from Eq. 2.7, a trend with a period longer

than 20 minutes is almost completely removed, while for a frequency greater than 0.05

cps the energy spectrum is practically not affected by the running average. The time-

series sample of 72,000 data points, representing the original analog data minus its

5-minute running average, was then used as an input to an IBM-7090 high-speed

computer for subsequent calculations of the correlation functions. A short sample of

turbulence and calibration wave reproduced from the digitized data is shown in Fig. 4.

The ordinate of the figure is in arbitrary computer units, representing velocity.

Superposed on the data is the sinusoidal calibration signal, through which the

absolute values of both velocity and time scale can be recovered.

3.0 DECAY OF WEAK TURBULENCE IN THE FINAL PERIOD

The main objectives of this study was to find how the kinetic energy of weak turbulences decay with time and how the turbulence-generating mechanism affect the final decay of such turbulences. It was found that in the final stage of decay the turbulence had equipartition of energy components and homogeneity in the cross-flow planes; see Section 2.2 and Fig. 2. This condition simplified the measurements that were required to describe such a field. That is, only one measurement of the longitudinal component of turbulence was sufficient for representing the field at each cross-flow section. A 35-minute recording of the turbulence was made at each different cross-flow plane, x distance from the grid. The data represent the turbulence at different decay times, $t = x/U$. The recorded data after being digitized and having their 5-minute running average removed were used to calculate $\overline{u^2}$ and various correlation functions.

The energy of turbulence for each record is calculated as

$$\overline{u_m^2} = \frac{\beta^2}{N} \sum_{h=1}^{N} e_h^2 \qquad (3.1)$$

where e_h is the digitized sample: β, the calibration constant; and N, the total number of digitized samples.

An estimate can be made on the normalized standard error due to limited record length, T_r, of the data. Assuming that the spectra of turbulence are approximately of white-noise type with band width, W, one finds that the normalized standard error was given by Bendat and Piersol[19] as

$$\epsilon = \frac{[Var(\overline{u^2})]^{1/2}}{\overline{u^2}} = (W T_r)^{-1/2} \qquad (3.2)$$

The band width of the turbulence is a function of the mean flow velocity, U, and a wave number, K_w, representing the cutoff wave number

$$W = \frac{K_w U}{2\pi}$$

where K_w for the present study (Fig. 10) is assumed to be $K_w [\nu (t-t_o)]^{1/2} = 0.50$. Since the dissipation length of turbulence is $\lambda = [5\nu(t-t_o)]^{1/2}$; see Section 5.0, then

$$\epsilon = \left[\frac{2\pi\lambda}{1.12 U T_r}\right]^{1/2} \tag{3.3}$$

For a mean velocity, U, the record length, T_r, has to be increased with increasing λ, if the same accuracy for obtaining the turbulence energy at different decay periods. $(t - t_o)$, is to be maintained. The maximum value for $(2\pi\lambda/1.12U)$ at the largest period of decay measured is of the order of 6 seconds (Fig. 8). For the fixed record length, T_r, of 30 minutes used in this experiment, the largest possible error ϵ is about 5.7 percent; at shorter decay periods near the grid, the error is negligible. Thus, the record period $T_r = 30$ minutes is considered adequate for the present investigation.

A small correction for the ambient noise was found necessary for the weak turbulence measured near the end of the channel. In general, the measured data ended when the ambient noise was more than 17 percent of the energy of turbulence. For every measured record of turbulence, the corresponding ambient noise of the same station was also recorded by removing the turbulence-generating grid. The noise

level was found to be nearly constant along the whole test channel. The same was true for the correlation function and the energy spectrum of the noise. Dye traces initiated at the upstream end of the channel were found to remain straight to the end of the channel. This indicated that there were no vortical velocity fields associated with the measured noise field; therefore, one may assume that these noises were due mainly to minute longitudinal oscillations of the channel flow and recorder noises. One may also assume that the noise fields were uncorrelated with the turbulence under study and could be subtracted from the measured data[14], as

$$\overline{u^2} = \overline{u_m^2} - \overline{u_n^2}$$
(3.4)

where $\overline{u_m^2}$ is the measured energy uncorrected for noise, and $\overline{u_n^2}$ is the energy of ambient noise.

In practice, the energy of turbulence was obtained as part of the computation for the autocorrelation function to be discussed in Section 4.0. The measured turbulence energies for different single grids were plotted in Fig. 5 as functions of the decay time t. The energy of turbulence created by the open Grid C approaches the inverse-square decay law at the very early stage of decay, while the turbulence energies for the two solid Grids A and B approach the same decay law at a later decay time. The data in Fig. 5 were replotted in linear scales as shown in Fig. 6. It is clear that $(U^2/\overline{u^2})^{1/2}$ varies linearly with t in the final period. This plot is used mainly to obtain the virtual origin of decay time, t_o, by extending the straight part of the energy curve toward the abscissa of time.

Further tests were conducted to see whether different initial conditions of the turbulence-generating process would affect the final decay law. This was done by using different combinations of multiple grids. One experiment consisted of a large solid Grid A placed 30.5 cm upstream of a small solid Grid B. The energy of turbulence was plotted in Fig. 5 against the decay time, t, in reference to the large Grid A. One notes that the energy of turbulence generated by Grid A was significantly reduced by the small Grid B. However, the turbulence in the final period followed the same inverse-square law. With the positions of the two grids interchanged, it is seen in Fig. 5 that there is no effect of the small grid on the large one. The decay time in this case is again in reference to the large Grid A. A third test involves a series of small identical small open Grids C. The spacing between these grids was varied between 4.8 and 9.8 M. The decay time is in reference to the downstream grid. It was found that in this case the turbulence generated by the three grids was exactly the same as that of one single grid. A similar trend was also observed by Tsuji and Hama[20] in their study of the initial period of turbulence decay behind multiple grids. However, the present experiment indicated that for weak turbulence produced by grids, the energy of such fields does not consist of waves that are independent and superposable but rather a field composed of a specific type of eddies.

In the experimental tests, it was found that multiple grids having nonintegral multiples of M/d ratios could cause a strong Moiré effect, i.e., large nonuniform drag effect. This results in large-scale eddies which could interact with the mean

flow field. For this case, the energy decay rate of turbulence was found to be less than the inverse-square law.

Attempts to create turbulence that would decay faster than the inverse-square law were not successful. All energy decay rates were either less than or equal to the inverse-square law. It should be noted that in order to obtain the observed inverse-square law, one has to achieve absolute uniformity in the mean flow field. If such a condition were not attained, the decay rate would always be less than the inverse-square. This may be the reason why such a decay rate is not commonly observed.

4.0 SELF-PRESERVATION OF CORRELATION FUNCTIONS AND ENERGY SPECTRA IN THE FINAL PERIOD

A correlation function for a weak turbulence field was first obtained by Batchelor and Townsend[13] in 1948. Since then no further work verifying the results has been known in the literature. This may be due largely to the fact that the technical difficulties involved in the measurement of weak turbulence were formidable. However, due to recent advances in both anemometry and data-processing techniques, studies of this nature are now possible.

In the present experimental setup, the turbulence under study is decaying in the mean flow direction. The effect of this longitudinal energy gradient is considered to have only minor effects on the basic decaying mechanism of the turbulence in its final period[8,12]. Hence, the mean velocity field may be considered as a carrier of turbulence. In computing the correlation functions and energy spectra, one may approximate the turbulence as being locally homogeneous. The digitized data for the fluctuating velocity component along the mean flow direction were used to compute the autocorrelation functions. From this the longitudinal correlation coefficients can be obtained by using the Taylor's approximation[1]. The one-dimensional energy spectra were computed directly from the Fourier transformation of the autocorrelation functions. Based on the assumption of local homogeneity and isotrophy, one may further compute the three-dimensional energy and dissipation spectra from the one-dimensional spectra.

The recorded data for the turbulence generated by a single Grid C and Grid B were used for detailed digital analysis. The analyzed data were further limited to the final period of decay, since the turbulence within this period was found to be plane homogeneous.

The autocorrelation function of $u(t)$ is defined as

$$R(\tau) = \lim_{T \to \infty} \frac{1}{T} \int_0^T u(t)\, u(t + \tau)\, dt \qquad (4.1)$$

which may be written in a discrete form for numerical computation

$$R_m = \frac{\beta^2}{N-m} \sum_{h=1}^{N-m} e_h\, e_{h+m} \qquad (4.2)$$

for $h = 1, 2, 3, \ldots, N$ and $m = 0, 1, 2, 3, \ldots, Q$.

where e_h is the discrete digitized sample after the 5-minute running average is removed from the original data; $\tau = m\Delta t$ is the correlation lag with sample interval Δt; N, the sample size; Q, the total discrete lag number; and β, the calibration constant. Note that $R(0) = R_{m=0} = \overline{u^2}$. The nondimensional time correlation is defined as

$$R_t(\tau) = \frac{R(\tau)}{R(0)} = \frac{R_m}{R_{m=0}}$$

In actual computation one has to choose a total lag, Q, which is more than large enough to cover the complete range of correlation function. After the first trial computation the required Q or maximum τ can be determined, so that for subsequent calculation Q can be reduced to a minimum in order to save computer time. The total correlation lag used in computing autocorrelations were $Q = 200$ or $\tau = 5$ seconds for Grid C, and $Q = 400$ or $\tau = 10$ seconds for Grid B.

An estimate for the normalized standard errors of the computed correlation function and energy spectrum[19] could be made if one assumes that the spectra of turbulence are approximately of white-noise type with band width, W, i.e.,

$$\epsilon_R = \frac{Var\,[R(\tau)]^{1/2}}{R(\tau)} = (2WT_r)^{-1/2}\,[\,1 + \frac{R^2(0)}{R^2(\tau)}\,]^{1/2} \tag{4.3}$$

The approximate band width of turbulence for this case is $(1.12\,U/2\pi\lambda)$; see Section 3.0, where U is the mean flow velocity, and λ is the dissipation length. At the longest period of decay for the present experiments, the value for $1/W$ is about 6 seconds; hence, for a record length, T_r, of 30 minutes, the largest standard error, ϵ_R, of the correlation function is

$$\epsilon_R = 0.04\,[\,1 + \frac{R^2(0)}{R^2(\tau)}\,]^{1/2}$$

One notes that at large τ where $R(0)/R(\tau)$ is not small the present measurements are not expected to be accurate. However, at small τ, the expected error is more acceptable. It should be noted that a tradeoff to make the present experiment more accurate must be made against computer time and capacity. In spite of the predicted large ϵ_R, the computed data show better consistency. The results of the normalized time-correlation functions, $R_t(\tau)$, at different stages of decay are shown in Figs. 7 and 8 for Grids C and B, respectively.

From the described results, one may re-examine more closely the condition of homogeneity[21] within the decaying field. For example, the gradients of length scales and energy in the mean flow direction must be small

$$\frac{dL_x}{dx} = \frac{L_x}{\lambda}\frac{d\lambda}{dx} = \frac{15}{2\mathbb{R}_\lambda}\left(\frac{\overline{u^2}}{U^2}\right)^{1/2} \ll 1 \qquad (4.4)$$

and

$$-\frac{L_x}{\overline{u^2}}\frac{d\overline{u^2}}{dx} = \frac{30}{\mathbb{R}_\lambda}\left(\frac{\overline{u^2}}{U^2}\right)^{1/2} \ll 1 \qquad (4.5)$$

where $\mathbb{R}_\lambda$ is the Reynolds number of turbulence; λ , the Taylor's dissipation length parameter; and L_x, the longitudinal integral length. These parameters are calculated and discussed in detail in Section 5.0. From the measured data we found that

$$0.01 < \frac{dL_x}{dx} < 0.025$$

and

$$0.04 < -\frac{L_x}{\overline{u^2}}\frac{d\overline{u^2}}{dx} < 0.1$$

Hence the fields may be considered to be locally homogeneous, and the Taylor's approximation[1] is applicable for the present experimental setup. It follows that the longitudinal correlation coefficient can be approximated by

$$f(r) = \frac{\overline{u(x+r)\,u(x)}}{\overline{u^2(x)}} = R_f(U\tau) \qquad (4.6)$$

where $r = U\tau$. The longitudinal correlation distant, r, is further normalized by the diffusion length parameter as

$$r^* = r\left[\nu(t-t_o)\right]^{-1/2} \qquad (4.7)$$

In the final period of decay the longitudinal correlation coefficients for both

Grid B and Grid C are found to have self-preserving form, as shown in Fig. 9. One

should note that this function is close to a Cauchy's distribution function, and is

definitely not of Gaussian type. It was found that in order to obtain the correct

dissipation and three-dimensional energy spectra from the correlation function one

must first obtain a precise one-dimensional spectrum through the Fourier transformation

of the longitudinal correlation coefficient . Since the spectra must cover an energy

range of at least 6 decades, see Fig. 10, it would be impractical to obtain such

spectra through direct measurements. The best solution at this stage is to attempt

to fit an analytical function over the measured self-preserving longitudinal-correlation

coefficient as shown in Fig. 9. A Cauchy's distribution function of the following

form was found to fit the correlation coefficient within experimental errors:

$$f(r^*) = \frac{1}{1 + (\frac{r^*}{\alpha})^2} \tag{4.8}$$

where α is the half width of the distribution function. The function with $\alpha = 3.2$

gives a perfect fit with the experimental data for $r^* < 10$, see Fig. 9. For $r^* > 10$

the fit is not as good. Since the values at large r^* will effect only the low frequency

spectra, they will have a small effect on the dissipation and the three-dimensional

spectra; and hence inaccuracy in this zone can be tolerated.

As discussed in the following section 5.0, the important nondimensional radius

of curvature, λ^*, for the longitudinal correlation function at $r^* = 0$ is directly related

to the energy decay rate of the system. The radius λ^* can be found directly from

Eq. 4.8 as:

$$\lambda^* = [-f''(0)]^{-1/2} = [\alpha^2/2]^{1/2} \tag{4.9}$$

According to the Kármán-Howarth equation 5.7 for a turbulent field whose energy

decays as $(t-t_o)^{-2}$ the value for λ^* should be equal to $\sqrt{5}$ or 2.24. Thus the

proper value for α in Eq. 4.9 should be equal to 3.16 instead of 3.2 according to the

best fitted curve. This coefficient will be shown later to have a strong influence on

the dissipation rate of turbulence. It was also found that the nondimensional correlation

functions have only a small change in functional form between the intermediate and

the final stages of decay.

From the analytical expression of the longitudinal correlation function one

can obtain the one dimensional spectrum through their Fourier transform relations.

$$E_1(K) = \frac{2\overline{u^2}}{\pi} \int_0^\infty f(r)\cos Kr \, dr \tag{4.10}$$

Here the power spectrum is defined in the positive wave number space so that

$$\overline{u^2} = A(t-t_o)^{-2} = \int_0^\infty E_1(K,t) \, dK \tag{4.11}$$

where A is a function of the geometry and the Reynolds number of the grid. Equations

4.10 and 4.11 can be nondimensionalized as follows:

$$E_1^* = \frac{E_1(K,t)(t-t_o)^{3/2}}{A \, \nu^{1/2}} = \frac{2}{\pi} \int_0^\infty f(r^*) \cos K^* r^* \, dr^* \tag{4.12}$$

where $K^* = K [\nu(t-t_o)]^{1/2}$

Substituting Eq. 4.8 into Eq. 4.12, one obtains the nondimensional one-dimensional

spectrum

$$E_1^* = \frac{2}{\pi} \int_0^\infty \frac{1}{1 + (\frac{r^*}{\alpha})^2} \cos K^* r^* \, dr^* = \alpha e^{-\alpha K^*} \tag{4.13}$$

This spectrum,also known as the Laplace's distribution function, is plotted in Fig. 10

for α equal to 3.16. It will be shown later that the decay rate of turbulence is

dictated primarily by the small variation at the vanishing end of the energy spectra;

and hence, the most important parameter governing this rate is the Taylor's dissipation

length λ . Henceforth we shall take $\alpha = 3.16$ as being the asymptotic value.

The nondimensional three-dimensional energy spectrum E* can be obtained

from the following transformation[22] of the one-dimensional spectrum, if the turbulent

field is homogeneous and isotropic,

$$E^* = \frac{E(t - t_0)^{3/2}}{A \, \nu^{1/2}} = \frac{K^{*3}}{3} \frac{d}{dK^*} [\frac{1}{K^*} \frac{dE_1^*}{dK^*}] = \frac{\alpha}{3} [K^* + \alpha K^{*2}] E_1^* \tag{4.14}$$

where E is the three-dimensional energy spectrum. It has been shown previously that

the present weak turbulence is approximately homogeneous and isotropic, except the

third-order correlation functions (see Section 6.0, Fig. 14) do not fully satisfy the

condition of local isotropy. Nevertheless, it is assumed that Eq. 4.14 is valid with

reservation. The self-preserving three-dimensional energy spectrum for the weak

turbulence is shown in Fig. 11. One notes that it peaks at about K* = 0.5 and vanishes to

a value of less than 0.01 at K* = 3, while the one-dimensional spectrum vanishes at

about K* = 1.8, see Fig. 10. It is clear that in order to obtain the correct three-

dimensional spectrum extreme accuracy is required in the one-dimensional spectrum.

Note also that E* is proportional to K* as K* → 0.

From the three-dimensional energy spectrum one can obtain the dissipation spectrum $D = 2\nu K^2 E$, which can be expressed in the nondimensional form as

$$D^* = \frac{D (t-t_o)^{5/2}}{A \, \nu^{1/2}} = -2 K^{*2} E^* \tag{4.15}$$

This function is shown in Fig. 12 for the case in which $\alpha = 3.16$. The dissipation spectrum peaks at $K^* = 1.2$ and vanishes at $K^* = 4.0$.

With these results one may proceed to examine the balance and transfer of energy among all of the wave number components. The time rate of change of energy[22] for a given wave can be expressed as

$$\frac{\partial E}{\partial t} = \Sigma (K,t) - 2\nu K^2 E \tag{4.16}$$

and the integrated rate of change of energy over all waves is

$$\int_0^\infty \frac{\partial E}{\partial t} \, dK = \int_0^\infty \Sigma(K,t) \, dK - \int_0^\infty 2\nu K^2 E \, dK = \frac{\overline{du^2}}{dt} = -2 A(t-t_o)^{-3} \tag{4.17}$$

where $\Sigma(K,t)$ is related to the triple correlation function representing the transfer of energy among the various waves. One notes that for the present case

$$\int_0^\infty \Sigma(K,t) \, dK = 0 \tag{4.18}$$

since no energy is generated or lost while the energy of waves are redistributed. Both Eqs. 4.16 and 4.17 can be nondimensionalized as

$$\left(\frac{\partial E}{\partial t}\right)^* = \Sigma^* + D^* \tag{4.19}$$

and
$$\int_0^\infty (\frac{\partial E}{\partial t})^* dK^* = \int_0^\infty D^* dK^* = -2 \tag{4.20}$$

Therefore
$$\Sigma^* = (\frac{\partial E}{\partial t})^* - D^*$$

Since
$$(\frac{\partial E}{\partial t})^* = -\frac{3}{2} E^* + \frac{K^*}{2} \frac{dE^*}{dK^*}$$

hence
$$\Sigma^* = \frac{\alpha K^*}{3} [2\alpha K^{*3} + (2 - \frac{\alpha^2}{2}) K^{*2} - \alpha K^* - 1] E_1^* \tag{4.21}$$

The energy transfer function is plotted in Fig. 12 for the case $\alpha = 3.16$. It is evident that the energy transfer function has a self-preserving and nonvanishing form, with continuous transfer of energy from low to high K^*. In other words, the waves are correlated throughout the final stage of decay, and they must be related to some specific types of physical vortices.

The integral of the dissipation spectra can be evaluated as

$$\int_0^\infty D^* dK^* = \int_0^\infty -\frac{2}{3} \alpha^2 [K^{*3} + \alpha K^{*4}] e^{-\alpha K^*} dK^* = -\frac{20}{\alpha^2} \tag{4.22}$$

The integral must equal -2, see Eq. 4.20, for the case in which $\overline{u^2} = A(t - t_o)^{-2}$.

Hence, α must equal to $\sqrt{10} = 3.16$ as is required by the Kármán-Howarth equation 5.2 mentioned before.

5.0   LENGTH PARAMETERS AND REYNOLDS NUMBER OF TURBULENCE

It is of general interest to find out how the various length parameters such as the Taylor's dissipation length parameter, λ , and the longitudinal integral length, L_x, and the Reynolds number of turbulence $\mathbb{R}_\lambda$, vary with the decay time.

The turbulence Reynolds number is defined as

$$\mathbb{R}_\lambda = \frac{(\overline{u^2})^{1/2}\lambda}{\nu} \tag{5.1}$$

where $(\overline{u^2})^{1/2}$ is the characteristic velocity; λ , the dissipation length parameter is taken as the characteristic length of turbulence, and ν is the kinematic viscosity.

The dissipation length parameter, λ , is defined by the Kármán-Howarth equation[3] at correlation distance equal to zero as

$$\frac{d\overline{u^2}}{dt} = - \frac{10\,\nu\,\overline{u^2}}{\lambda^2} \tag{5.2}$$

If the decay of the kinetic energy of turbulence follows a simple power law of the form $\overline{u^2} \propto (t-t_o)^{-2}$, the dissipation length parameter may be written as

$$\lambda = [5\nu(t-t_o)]^{1/2} \tag{5.3}$$

since $t_o \ll t$ in the final period, this approximation is a valid one to use. The parameter λ may also be evaluated, as mentioned before, from the radius of the longitudinal correlation coefficient $f(r)$ near the origin, i.e.,

$$-f''(r=0) = 1/\lambda^2 \tag{5.4}$$

The numerical evaluation of λ from $f''(0)$ was made by the least-square fitting of power series of r through $f(r)$ near the origin and solving for the radius of curvature at $r = 0$. It was found that λ evaluated by this method was quite close to the Kármán-Howarth approximation of λ in the final period of decay. Before the final period, λ can only be obtained from the radius of curvature of $f(r)$ at $r = 0$.

The longitudinal integral length, L_x, may be computed from the following definition:

$$L_x = \int_0^\infty f(r)\,dr \tag{5.5}$$

It was found numerically that $L_x \doteq 2\lambda$.

The Reynolds number of turbulence in the final period may be estimated by

$$R_\lambda = \frac{(\overline{u^2})^{1/2}\lambda}{\nu} = \left[\frac{5(t-t_0)\overline{u^2}}{\nu}\right]^{1/2}$$

while R_λ before the final period is computed directly from

$$R_\lambda = \frac{1}{\nu}\left[\frac{\overline{u^2}}{f''(0)}\right]^{1/2} \tag{5.6}$$

The measured R_λ and λ are presented in Fig. 13. It is interesting to note that for the case of open Grid C, the Reynolds numbers of turbulence are under 30, and the decay of energy follows the inverse-square law at a very early stage. However, for the two solid Grids, A and B, the initial Reynolds numbers of turbulence are more than 50. As R_λ decreased to approximately 30, the decay of energy was found to approach the inverse-

square law, and followed the law throughout the last period. In the present experimental

setup, the onset of the inverse-square law is approximately $\mathbb{R}_\lambda \leq 30$.

6.0 THIRD AND FOURTH-ORDER CORRELATION FUNCTIONS

The correlation functions of the third and the fourth orders are the additional

statistical characteristics of the turbulent field which are of direct interest to the

statistical theory of turbulence.

The time-correlation coefficients[23] of higher order are defined as

$$R_t^{m,n}(\tau) = \frac{\overline{u^m(t)\, u^n(t+\tau)}}{[\overline{u^2(t)}]^{(m+n)/2}} \qquad (6.1)$$

If the joint-probability density distribution of velocities is assumed to be Gaussian,

then the correlation coefficients of higher order that are even are given by a function

of the second-order correlation coefficients [23] $R_t(\tau)$, and the correlation coefficients

of odd order are all zero. This may be subjected to experimental verification.

The measured correlation coefficients of the third and fourth orders at various

stages of decay were compared with results of Frenkiel and Klebanoff[23] in Fig. 14.

The data used for computing the correlation coefficients of the third and fourth orders

are based on those of the small open Grid C with measurements taken at positions ·

x/M = 4.8 and 19.2. As shown in Fig. 14, the measured correlation coefficients

of the third order are very similar to those of Frenkiel and Klebanoff . In the case

of isotropic turbulence, $R_t^{2,1}(\tau)$ should be equal to $-R_t^{1,2}(\tau)$, and third order moment

coefficient, $\overline{u^2(t)}/[\overline{u^2(t)}]^{3/2}$, should be equal to zero. The present results for weak

turbulence and the results of Frenkiel and Klebanoff at higher Reynolds numbers

emphasize that turbulence produced by grids is not exactly isotropic, since

$$R_t^{2,1}(\tau) \neq -R_t^{1,2}(\tau)$$

and

$$R_t^{2,1}(0) = R_t^{1,2}(0) \neq 0$$

The fact that the third-order moment coefficient is not zero also implies that the waves are not completely independent.

If the time skewness[23] is written as

$$S_t^3(\tau) = 3[R_t^{2,1}(\tau) - R_t^{1,2}(\tau)] \qquad (6.2)$$

it is noted that the maximum time skewness at two different stages of decay (Fig. 14) is approximately at $2 \wedge$.

If the Gaussian probability density distribution of turbulence velocities is assumed, the fourth-order correlations can be represented by the second-order correlation[23], i.e.,

$$R_t^{1,3} = R_t^{3,1} = 3R_t \qquad (6.3)$$

and

$$R_t^{2,2} = 1 + 2(R_t)^2 \qquad (6.4)$$

The experimentally measured fourth-order correlations are compared with the corresponding Gaussian values calculated by using Eqs. 6.3 and 6.4 for $R_t^{1,3}$, $R_t^{3,1}$, and $R_t^{2,2}$ from the measured second-order correlation coefficients, R_t, in Fig. 7. As shown in Fig. 15, the measured fourth-order correlation coefficients depart from the predicted curves at regions of small lag.

7.0 COMPARISON WITH STATISTICAL THEORY OF TURBULENCE

On the basis of the theoretical result of Diessler (Fig. 3 of Ref. 8) and also of Lee and Tan[12], the effects of longitudinal inhomogeneity of the present grid-produced weak turbulence on the spectrum tensor are negligible. Thus, the statistical theory[6,11,13,24] for the weak homogeneous turbulence can be used to compare against the measured data. Before making such comparisons, a brief review of the statistical theory of turbulence is desirable. The Navier-Stokes equations for the weak homogeneous turbulence field are in the form of

$$\frac{\partial u_i}{\partial t} + u_j \frac{\partial u_i}{\partial x_j} = -\frac{1}{\rho}\frac{\partial p}{\partial x_i} + \nu \nabla^2 u_i \tag{7.1}$$

where u_i and p are the fluctuating velocity components and pressure, respectively, and the constants ρ and ν are mass density and kinematic viscosity of the fluid, respectively. If we multiply Eq. 7.1 by u_j and add to the product a similar equation with i and j interchanged, the resultant two-point correlation equation is

$$\frac{\partial}{\partial t} R_{ij}(r, t) = S_{ij}(r, t) + 2\nu \nabla^2 R_{ij}(r, t) \tag{7.2}$$

where

$$R_{ij}(r, t) = \overline{u_i(x, t)\, u_j(x+r, t)}$$

and

$$S_{ij}(r, t) = O_2 \{ \frac{\partial}{\partial x_k} \overline{u_i(x,t)\, u_j(x+r,t)\, u_k(x,t)} + \frac{1}{\rho}\frac{\partial}{\partial x_i} \overline{p(x,t)\, u_j(x+r,t)} \}$$

Here the operator O_2 acting on a second-order tensor $C_{ij}(r)$ is

$$O_2 \{C_{ij}\} = C_{ij}(r) + C_{ji}(-r)$$

One may take Fourier transformation of Eq. 7.2 by defining

$$\Phi_{ij}(K,t) = \int\!\!\!\int\!\!\!\int_{-\infty}^{\infty} R_{ij}(r,t)\, e^{i\vec{K}\cdot\vec{r}}\, \vec{dr}$$

and

$$\Sigma_{ij}(K,t) = \int\!\!\!\int\!\!\!\int_{-\infty}^{\infty} S_{ij}(r,t)\, e^{i\vec{K}\cdot\vec{r}}\, \vec{dr}$$

Then one obtains the spectrum tensor equation from Eq. 7.2

$$\frac{\partial}{\partial t}\Phi_{ij}(K,t) = \Sigma_{ij}(K,t) - 2\nu K^2 \Phi_{ij}(K,t) \tag{7.3}$$

It is clear that the two-point correlation and spectrum tensor equations are indeterminate since the terms $S_{ij}(r,t)$ and $\Sigma_{ij}(K,t)$ are completely unspecified. Equations for $S_{ij}(r,t)$ can be obtained; however, these involve the fourth-order correlations, and so on.

In the final period of decay, $S_{ij}(r,t)$ and $\Sigma_{ij}(K,t)$ are assumed negligible; then we have

$$\frac{\partial}{\partial t}R_{ij}(r,t) = 2\nu \nabla^2 R_{ij}(r,t) \tag{7.4}$$

and

$$\frac{\partial}{\partial t}\Phi_{ij}(K,t) = -2\nu \nabla^2 \Phi_{ij}(K,t) \tag{7.5}$$

Equation 7.5 possesses a solution of the form

$$\Phi_{ij}(K,t) = \Phi_{ij}(K,t_o)\, e^{-2\nu K^2(t-t_o)} \tag{7.6}$$

The equations of motion do not supply the initial spectrum tensor, $\Phi_{ij}(K,t_o)$,

although they must obey continuity and the condition of symmetry, i.e.,

$$K_i \Phi_{ij}(K,t_o) = K_j \Phi_{ij}(K,t_o) = 0 \qquad (7.7)$$

and

$$\Phi_{ij}(K,t_o) = \Phi_{ji}(-K,t_o) \qquad (7.8)$$

As $(t-t_o) \to \infty$, the exponential factor will be small except for small values of K,

then one can replace $\Phi_{ij}(K,t_o)$ by the Taylor's expansion of $\Phi_{ij}(K,t_o)$ about $K = 0$.

This expansion satisfies Eqs. 7.7 and 7.8 and is defined as a class of admissible initial

spectra. When the turbulence is isotropic, the foregoing results can be greatly

simplified. The isotropic three-dimensional energy spectrum, $E(K,t) = 2\pi K^2 \Phi_{ii}(K,t)$

is given by

$$\frac{\partial}{\partial t} E(K,t) = -2\nu K^2 E(K,t) \qquad (7.9)$$

and

$$E(K,t) = E(K,t_o) e^{-2\nu K^2(t-t_o)} \qquad (7.10)$$

Equations 7.5 and 7.9 indicate that the energy components coming from different wave

numbers are statistically independent. By the Taylor's expansion of initial spectrum,

$E(k,t_o)$, about $K = 0$, one can find a class of admissible solutions for $E(K,t)$ that is

consistent with the Navier-Stoke equation (Eq. 7.1), continuity (Eq. 7.7), and the

condition of symmetry for the spectrum tensor (Eq. 7.8). The admissible solutions of

the spectrum[11,12] for the homogeneous and isotropic weak turbulence are in the

form of

$$E_s(K,t) = J_s K^s e^{-2\nu K^2(t-t_o)} \qquad (7.11)$$

for s = 2,3,4 ... , where J_s is a constant. This leads to a total decay of energy in

the final period of the following form:

$$\overline{u^2} = \int_0^\infty E_s(K,t)\,dK = J_s \frac{\Gamma[(s+1)/2]}{(2\nu t)^{(s+1)/2}} \qquad (7.12)$$

It is apparent that considerable variety in the ultimate decay of turbulence can be

obtained by choosing different admissible initial spectra.

The self-preserving form for the admissible solution of the spectrum can be

obtained by rewriting Eq. 7.11, i.e.,

$$E_s \,\nu^{-1/2}(t-t_o)^{s/2} = \frac{J_s}{\nu^{(s+1)/2}} [\nu K^2(t-t_o)]^{s/2} e^{-2\nu K^2(t-t_o)} \qquad (7.13)$$

The dimensionless plots of $E_s \,\nu^{-1/2}(t-t_o)^{s/2}$ versus K^* for all the admissible

solutions possess a self-preserving "bell shape" with $E_2 \,\nu^{-1/2}(t-t_o)$, $E_3 \,\nu^{-1/2}(t-t_o)^{3/2}$

and $E_4 \,\nu^{-1/2}(t-t_o)^2$ peaking at K^* equal to 1.00, 0.866, and 0.707,

respectively.

The longitudinal correlation functions corresponding to the admissible solutions

given by Birkoff[11] are

$$f_4(\frac{r}{\lambda}) = e^{-r^2/2\,\lambda^2} \qquad (7.14)$$

corresponding to $E_4(K,t) = J_4 K^4 e^{-2\nu K^2(t-t_o)}$, and $\overline{u^2} \infty (t-t_o)^{-5/2}$;

$$f_3(\frac{r}{\lambda}) = \frac{4\lambda^2 + 5r^2}{5r^2} \sqrt{\frac{4}{5}} \lambda \int_0^\infty e^{-(2/5)K^2 \lambda^2} \sin K r \, dK - \frac{5\lambda^2}{4r^2} \qquad (7.15)$$

corresponding to $E_3(K,t) = J_3 K^3 e^{-2\nu K^2(t-t_o)}$, and $\overline{u^2} \infty (t-t_o)^{-2}$;

and $$f_2(\frac{r}{\lambda}) = \frac{3^{5/2} \lambda^3}{5^{3/2} r^3} \{ \sqrt{\pi/2} \operatorname{erf}(\sqrt{5/3} \frac{r}{\lambda}) - \sqrt{5/3} \frac{r}{\lambda} e^{-5r^2/6 \lambda^2} \}$$

$$(7.16)$$

corresponding to $E_2 = J_2 K^2 e^{-2\nu K^2(t-t_o)}$, and $\overline{u^2} \infty (t-t_o)^{-3/2}$.

Here we have normalized r by the dissipation length $\lambda = [20\nu(t-t_o)/(s+1)]^{1/2}$ which is the curvature of the longitudinal correlation function, $f_s(r)$, near the origin of r = 0.

As shown in Fig. 5, the kinetic energy of turbulence decays as the inverse-square of time for all cases tested. Although the inverse-square decay law is one of the admissible solutions of the normal statistic of weak turbulence, the measured longitudinal correlation coefficients and the energy spectrum should also be in agreement with those corresponding to the inverse-square decay law predicted by the existing theory. For large correlation distance, the longitudinal correlation coefficient, f_3, corresponding to the inverse-square decay law, should be slightly larger than the curve

f_4, corresponding to the -5/2 power law, and slightly less than f_2 corresponding to the -3/2 power law. As shown in Fig. 9, the present measured longitudinal correlation coefficient, $f(r)$, is not only larger than f_3 but also larger than f_2 as predicted by the existing theory. Also the three-dimensional energy spectrum peaks at $K^* = 0.5$ as predicted. Consequently, the energy transfer function is not zero at the final stage of decay but plays an important role in the mechanics of decay.

In general, the experimental results are not in full agreement with the results of existing theories for weak turbulence. The statistical theory of turbulence according to Birkhoff[11] is characterized by

1. Quantities depending linearly on the velocity field being normally distributed, and

2. Components coming from different wave number vectors being statistically independent (Eqs. 7.5 and 7.9).

Under normal statistics all odd-order correlations should vanish and the fourth-order moment coefficient should be equal to 3. It was found that the measured third and fourth-order correlation functions were not consistent with Statement 1. As shown in Fig. 14 and 15, the third-order moment coefficient, $\overline{u^3}(t)/[\overline{u^2}(t)]^{3/2}$, is between 0.06 and 0.1, and the fourth-order moment coefficient, $\overline{u^4}(t)/[\overline{u^2}(t)]^2$, is not quite equal to 3. The assumption of a Gaussian joint-probability distribution of velocities is also not quite valid. Furthermore, since the measured energy transfer function (Fig. 12) and consequently the second-order correlation function (Fig. 9) are not in agreement with those assumed by the existing theories, Statement 2 is not consistent with the present measurements.

8.0 COMPARISON WITH KINETIC MODEL

Visual observation of the perturbation of capillary dye traces in all grid-produced weak turbulence showed a distinctive turbulent field structure consisting of noninteracting, randomly orientated, aged vortices identical to those reported by Tan and Ling[14]. No detectable change in the basic structure of turbulence was observed even down to the very last stage of decay, which was no longer measurable by the instruments. For all cases tested, the energy of turbulence decayed precisely as $(t-t_0)^{-2}$ in the final period (Fig. 5), which was consistent with the kinetic model. Thus, it is interesting to discuss the kinetic model in relationship to the present experimental data.

The turbulence field in the final period of decay may be considered as a field consisting of essentially noninteracting, aged line vortices with limited distribution in energy and size. In the absence of a mean shear field, the probability distribution of the vortices in space should be uniform and the orientation of the vortices should be completely random. The main feature of such a field is dominated by the physical line eddies, whose energy decay rate is independent of size. The velocity field of a line vortex of finite energy is best described by the Rouse-Hsu[25] model, i.e.,

$$V = \frac{H}{2\pi r} [\, e^{-\frac{r^2}{\sigma a + 4\nu t}} - e^{-\frac{r^2}{a + 4\nu t}} \,] \qquad (8.1)$$

It is important to note that the velocity field is a solution of the Navier-Stokes equation, where r in Eq. 8.1 is the distance from the vortex center. The constants H, a, and σ

are related to the initial field characteristics[23] r_o, Γ_o , and ζ_o as

$$r_o = \{[\sigma a/(\sigma - 1)] \ln \sigma\}^{1/2}$$

$$\Gamma_o = H(\sigma - 1) \sigma^{\sigma/(1-\sigma)}$$

$$\zeta_o = H(\sigma - 1)/\pi \sigma a$$

where r_o is the initial radius of maximum circulation Γ_o; ζ_o , the initial

centerline vorticity; $a = 4\nu t_d$; t_d, the initial decay time (ahead of $t = 0$);

$\sigma = 1 + t_g/t_d$; and t_g is the time of vortex generation.

The kinetic energy per unit length of vortex is

$$K.E. = \pi \rho \int_0^\infty V^2 r \, dr$$

(8.2)

$$- \frac{\Gamma^2}{8\pi} \cdots \cdots \frac{4 \nu^2 t^2}{(\sigma a + 4 \nu t)(a + 4 \nu t)}$$

In the final period of decay, $t_d + t \gg t_g$; thus, the asymptotic expansion of the

energy decay becomes

$$K.E. = \frac{\rho H^2 t_g^2}{32 \pi} (t_d + t)^{-2} \sim A(t + t_d)^{-2}$$

(8.3)

Tan and Ling[14] have shown that the statistical average of the turbulence kinetic

energy in plane $\Sigma(t)$ decays with $(t + t_d)^{-2}$, according to the same decay law as

an individual eddy, provided the latter does not depend on the eddy scale. It is clear

that this decay law is not affected by the inherent initial conditions.

The typical length scales of the single vortex are the core sizes of the maximum

velocity and the maximum circulation at any time in the final period. Let ξ and η be

the radii of the maximum velocity and the maximum circulation of the vortex, respectively.

Then at $r = \xi$, $\partial V/\partial r = 0$, and at $r = \eta$, $\partial r V/\partial r = 0$. Thus

$$\frac{a(\sigma - 1)\xi^2}{(\sigma a + 4\nu t)(a + 4\nu t)} = \ln \{1 + \frac{2\xi^2(\sigma - 1)a}{(\sigma a + 4\nu t)(a + 4\nu t) + 2\xi^2(a + 4\nu t)} \}$$

and

$$\frac{a(\sigma - 1)\eta^2}{(\sigma a + 4\nu t)(a + 4\nu t)} = \ln \{1 + \frac{(\sigma - 1)a}{a + 4\nu t} \}$$

Again assume that $t_d + t \gg t_g$ in the final period, then the asymptotic expansion of ξ and η are

$$\xi = \sqrt{2}\, [\nu(t - t_d)]^{1/2} = 0.63\,\lambda \qquad (8.4)$$

$$\eta = 2[\nu(t - t_d)]^{1/2} = 0.89\,\lambda \qquad (8.5)$$

It is important to note that the Taylor's dissipation length is of the order of ξ . If the weak turbulent eddies generated by a grid are considered as noninteracting, randomly orientated, aged vortex elements, the typical length scale of the weak turbulent eddies is always proportional to the length scale of the single vortex. The length scales of a single vortex in the final period is $\xi \sim \eta \sim [\nu(t - t_o)]^{1/2}$, where t_d is taken to be of the order of t_o. If the spectral function in the final period possesses a self-preserving form, it may be written as

$$E_1(K, t) = F\{\nu, (t - t_o)\}\, \psi\{K\,[\nu(t - t_o)]^{1/2}\} \qquad (8.6)$$

where E_1 is the longitudinal one-dimensional energy spectrum and $\psi\{K^*\}$ is a

similarity function. The total energy is

$$\int_0^\infty E_1(K,t)\,dK = \int_0^\infty \frac{F\{\nu,(t-t_0)\}}{[\nu(t-t_0)]^{1/2}}\,\psi\{K^*\}\,dK^*$$

$$= \overline{u^2} = A(t-t_0)^{-2}$$

Thus

$$F\{\nu,(t-t_0)\} = \frac{A\,\nu^2[\nu(t-t_0)]^{-3/2}}{\int_0^\infty \psi\{K^*\}\,dK^*} = C\,\nu^{1/2}(t-t_0)^{-3/2} \quad (8.7)$$

where $K^* = K[\nu(t-t_0)]^{1/2}$, and C is a constant. The measured self-preserving

form of the one-dimensional energy spectra shown in Fig. 10, confirms the

normalizing function for the spectral energy.

The correlation and spectral functions based on the kinetic model have not

yet been developed. However, since the measured spectral and correlation functions

are different from those based on the normal statistics, it would imply that the

statistical structure of a weak turbulence field has a limited degrees of freedom. That

is, the field has some preferred structures in the form of aged physical line-eddies.

In general, the correlation function is directly related to the eddy structure, i.e.,

the velocity fields at two points within an eddy are correlated, while those without

an eddy are uncorrelated. Since the physical eddies are not spherical in structure,

they would contribute to a correlation function having broader shape, and a three-

dimensional spectral-function peaking at lower wave numbers, similar to those observed

experimentally. In addition, the wave components from such a field are expected to

be correlated in part as indicated by the experimental results.

9.0 CONCLUSIONS

By comparing the experimental results with the existing statistical theories and the kinetic model of a weak turbulent field, one may draw the following conclusions:

1. The kinetic energy of weak turbulence generated by single-biplane and multiple-stage grids was found to decay in the final period precisely as the inverse-square of the decay time. The energy of the weak turbulence produced by multiple stages of grids does not follow the simple superposition principle. This implies that the weak turbulence is not composed of independent waves but a field that has a definite preferred structure which controls the mechanics of decay.

2. Although the inverse-square decay law is one of the admissible solutions of the statistical theory of weak turbulence, both the measured second-order correlation and the energy transfer functions are not consistent with those assumed under normal statistics. This inconsistency implies also that the wave components coming from a field of definite structure are not completely random with unlimited degrees of freedom. Experimental results indicated continuous transfer of energy from low to high wave numbers throughout the final stage of decay.

3. The measured third-order moment coefficient, $\overline{u^3}(t)/[\overline{u^2}(t)]^{3/2}$, is approximately equal to 0.1; the measured fourth-order moment coefficient, $\overline{u^4}(t)/[\overline{u^2}(t)]^2$, is not quite equal to 3; and the assumption of a Guassian joint-probability distribution of velocities is also not quite valid with regard to the third and fourth-order correlations especially at small lags. These results are contradictory to the assumption that quantities linearly related to the velocity field are normally distributed.

4. When the Reynolds number of turbulence was less than 30, the energy of turbulence was found to decay as the inverse-square of time. In this final period of decay, all turbulence length scales were found to increase as the square root of decay time, while the Reynolds number of turbulence was found to decrease with the inverse-square root of time. The measured longitudinal correlation coefficients are close to the Cauchy's distributions, and they possess a self-preservative form with respect to $r[\nu(t-t_o)]^{-1/2}$. Both the measured Taylor's dissipation length and the integral of dissipation spectrum correspond well with the observed decay rate of turbulence.

5. Through visual observation of the perturbations of capillary dye streaks, the turbulent field in the final period of decay was found to be also characterized by aged and essentially noninteracting line vortices. No further change in the basic structure of turbulence was observed down to the last perceptible perturbation of the dye streaks. Thus, all experimental evidence indicated that a weak homogeneous turbulence has a definite preferred structure.

REFERENCES

1. G.I. Taylor, Proc. Royal Soc. (London) A 151, 421 (1935); A 156, 307 (1937); A 164, 15 (1938); A 164, 476 (1938).

2. M. Millonshtchikov, Comptes Rend. Acad. Sci., U.R.S.S. 22, 236 (1939); Comptes Rend. Acad. Sci. U.R.S.S. 22, 231 (1939).

3. Th. Von Karman and L. Howarth, Proc. Roy. Soc. (London) A 164, 92 (1938).

4. L.G. Loitsiansky, Central Aeronautics and Hydrodynamics Institute (Moscow) Report 440 (1939).

5. C.C. Lin, Proc. of the Seventh International Congress on Applied Mechanics (Allen and Unwin, London) 2, p. 127 (1948).

6. G.K. Batchelor, Proc. Roy. Soc. (London) A 195, 513 (1949).

7. S. Chandrasekhar, Phil. Trans. Roy. Soc. (London) A 557, 242 (1955)

8. R.G. Deissler, Phys. Fluids 4, 1187 (1961).

9. O.M. Phillips, Cambridge Phil. Society Proceedings A, 52 (1956).

10. P.G. Saffman, Journal of Fluid Mechanics, 27, 581 (1967).

11. G. Birkhoff, Communs. Pure Appl. Math. 7, 19 (1954).

12. D.A. Lee and H.S. Tan, Physics of Fluids 10, 1224 (1967).

13. G.K. Batchelor and A.A. Townsend, Proc. Roy. Soc. (London) A 194, 527 (1948).

14. H.S. Tan and S.C. Ling, Physics of Fluids 6, 1693 (1963).

15. R.G. Deissler, Physics of Fluids 8, 2106 (1965).

16. G.K. Batchelor and R.W. Stewart, Quarterly Journal, Mech. Appl. Math. 3, 1 (1950).

17. S.C. Ling, Journal of Basic Engineering, ASME, 82, 629 (1960).

18. R.B. Blackman and J.W. Tukey, The Measurement of Power Spectra (Dover, 1959).

19. J.S. Bendat and A.G. Piersol, Measurement and Analysis of Random Data, 1958 (John Wiley and Sons, Inc.)

20. H. Tsuji and F.R. Hama, Journal of Aeronautical Sciences, 20, 848 (1953).

21. S. Corrsin, Handbuck der Physik, Springer-Verlag (Berlin, Germany), 8, 530 (1963).

22. C.C. Lin, Turbulent Flows and Heat Transfer, Princeton Univ. Press, 212 (1959).

23. F.N. Frenkiel and P.S. Klebanoff, Physics of Fluids 10, 507 and 1737 (1967).

24. R.G. Deissler, Physics of Fluids 3, 176 (1960).

25. H. Rouse and H.C. Hsu, Proc. of the First U.S. National Congress of Applied Mechanics, ASME, 741 (1950).

Speed-regulated motor

Baffle plate

Critical flow

Inlet scroll cage

Pump

DETAILS OF PUMP

Biplane grid

Flow

1100 cm

FRONT VIEW

99 cm

Baffle plate

Marine fiberglass plastic

Marine plywood

60 cm

10,2 cm Pipes

60 cm

39 cm

SECTION A - A

Damping screens and Honeycombs

DETAILS OF INLET END

Fig. 1   Water Channel

○ $\mathbb{R}_M = 470$, M = 0.78cm, M/d = 2.8, U = 2.9 cm/sec
□ $\mathbb{R}_M = 940$, M = 0.56cm, M/d = 2.8, U = 2.9 cm/sec
△ $\mathbb{R}_M = 840$, M = 0.18cm, M/d = 5.0, U = 2.9 cm/sec

1.25
1.20
1.15
1.10
1.05
1.00
0.95
0.90
0.85

$\dfrac{\overline{U^2}}{\overline{V^2}}$

0   20   40   60   80   100   120   140   160   180   200   220   240   260   280   300

x/M

Fig. 2   Equipartition of the Energy Components of Weak Turbulence
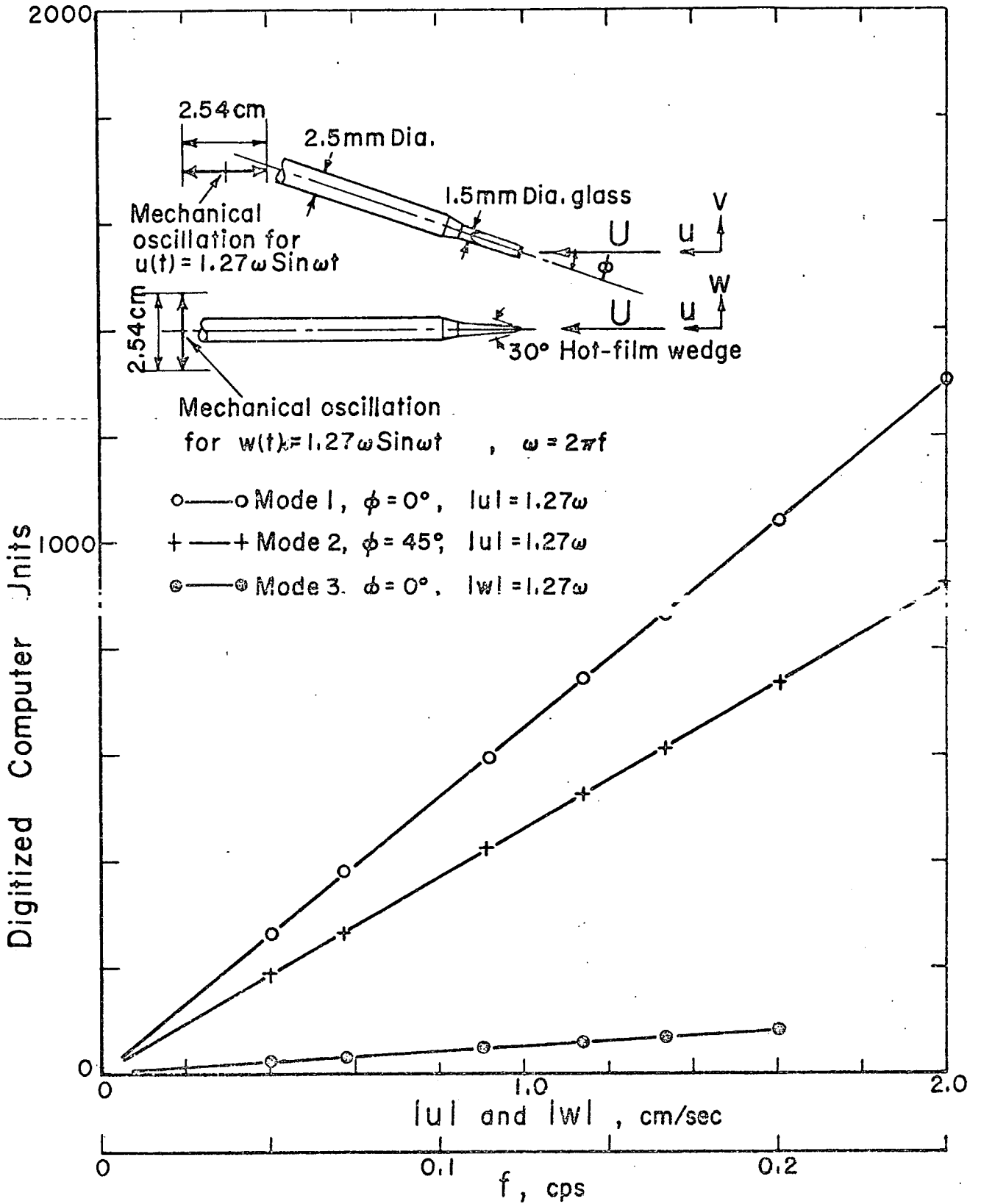
Fig. 3   Typical Calibration Curves for Hot-Film Probe

53
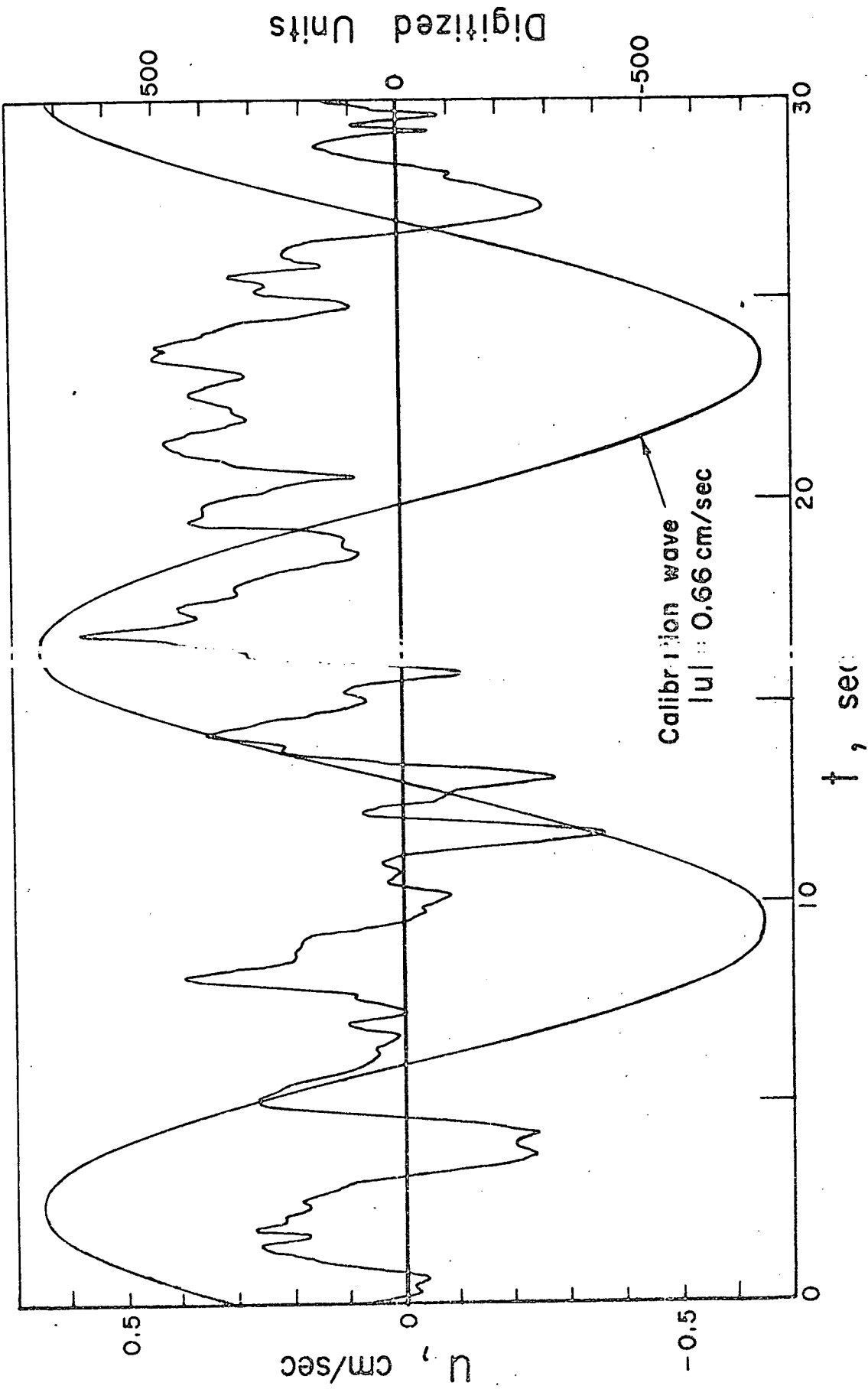
Fig. 4 Reproduced Sample of Digitized Turbulence and Calibration Wave
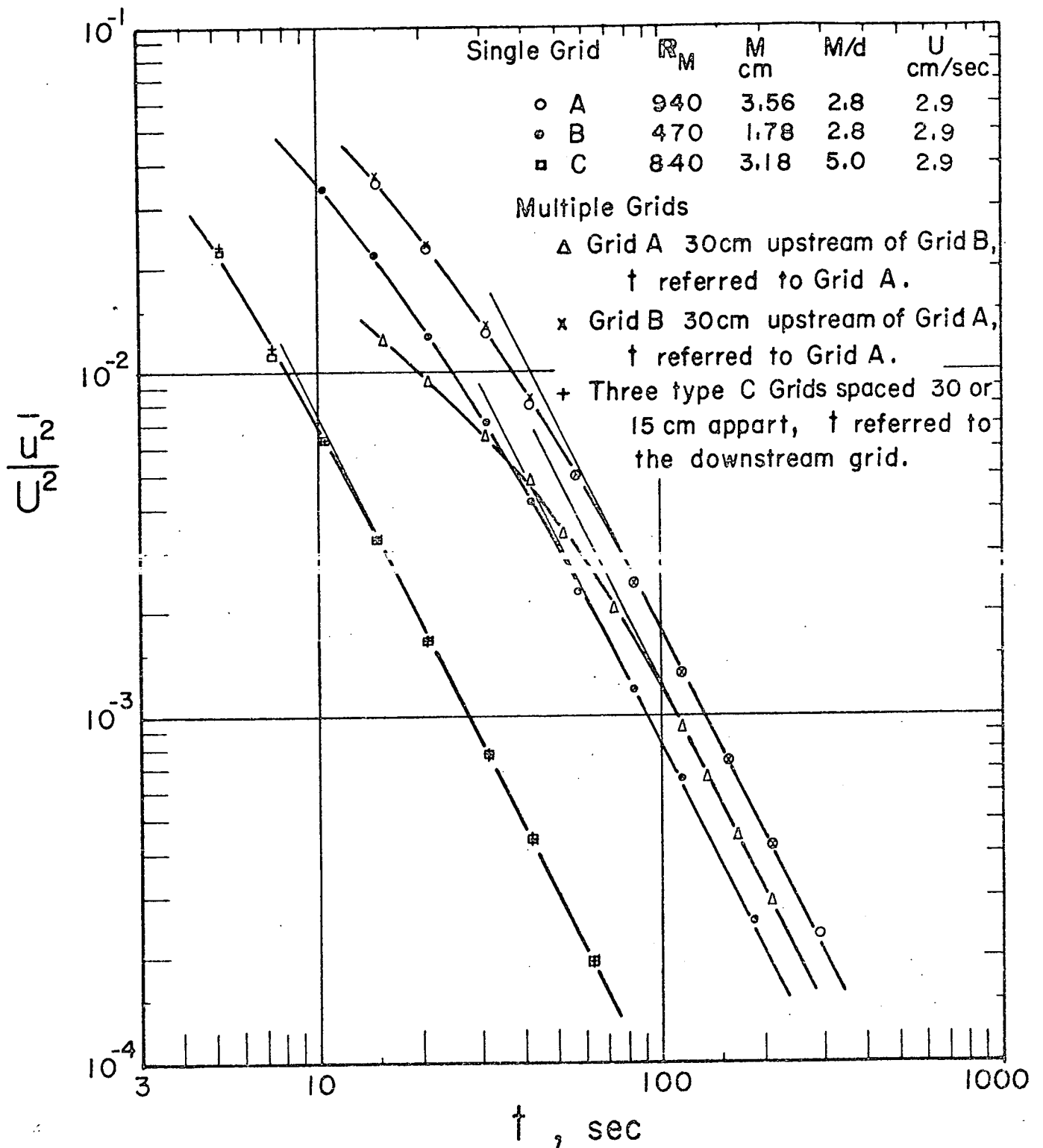
Fig. 5   Energy Decay of Weak Turbulence

Grid	t_o
A	-14 sec
B	-12
C	-2
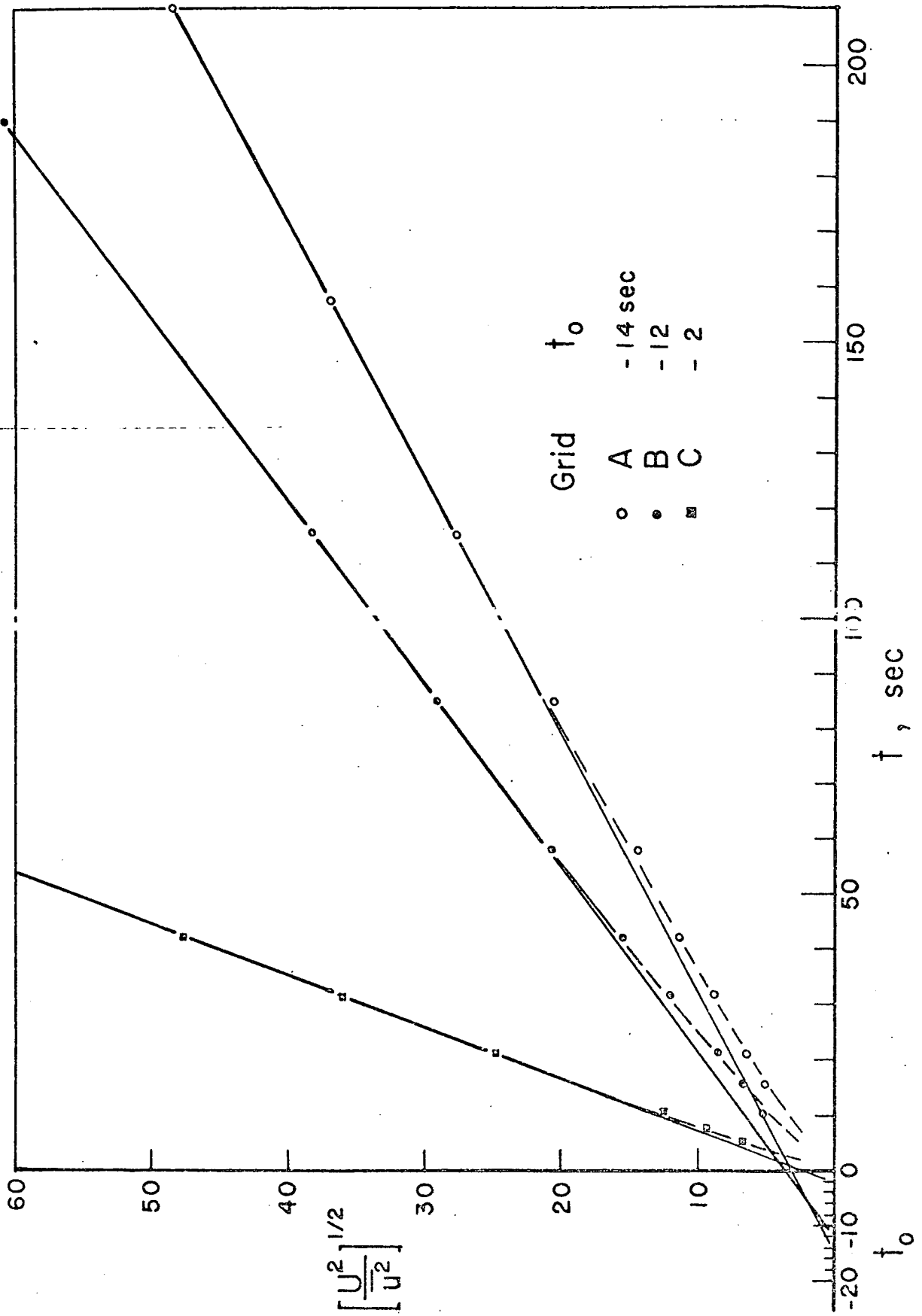
Fig. 6   Linear Plot of Energy Decay for Defining the Virtual Origin of Decay Time
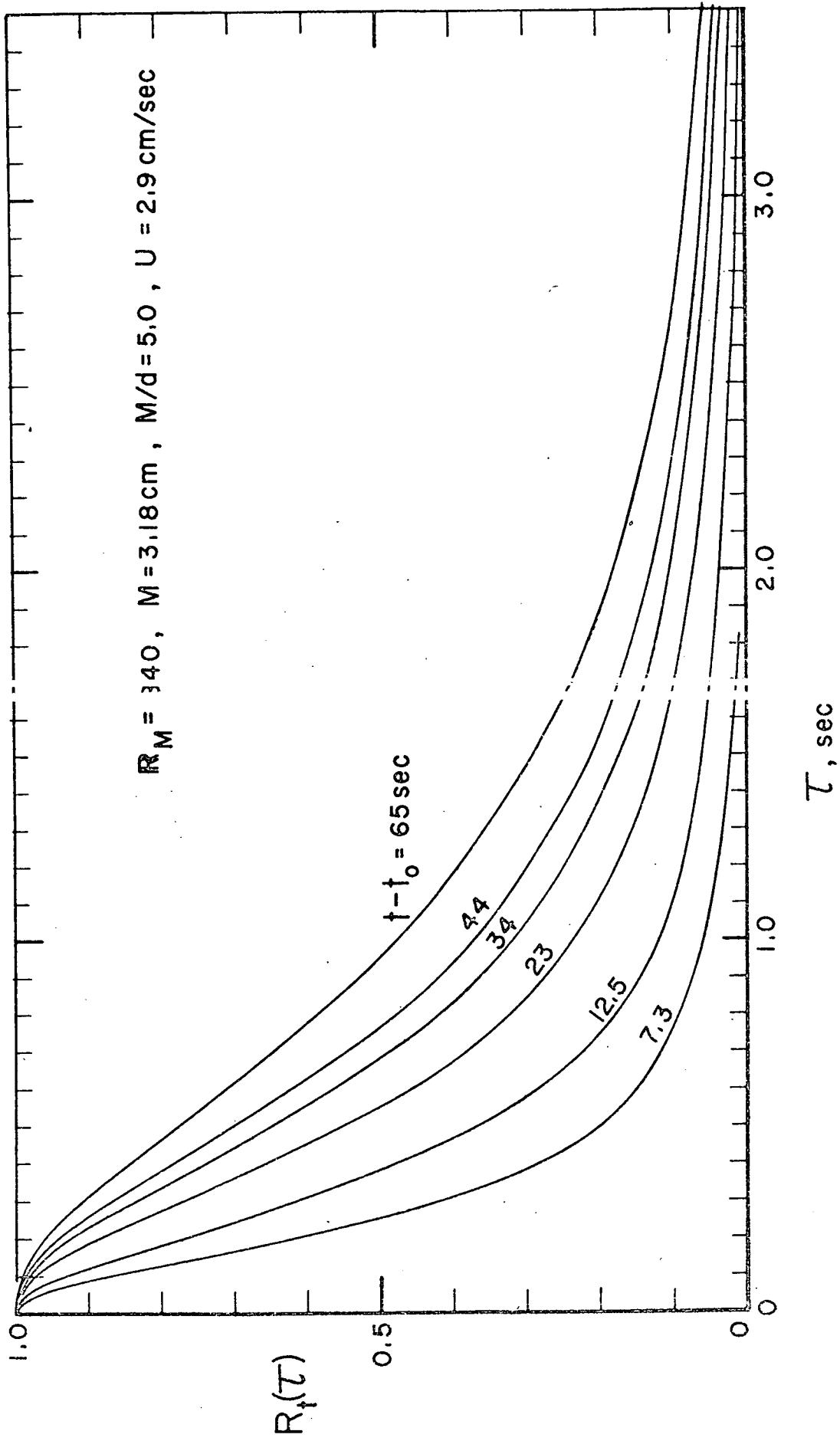
Fig. 7   Time-Correlation Coefficient at Different Stages of Decay (Grid C)
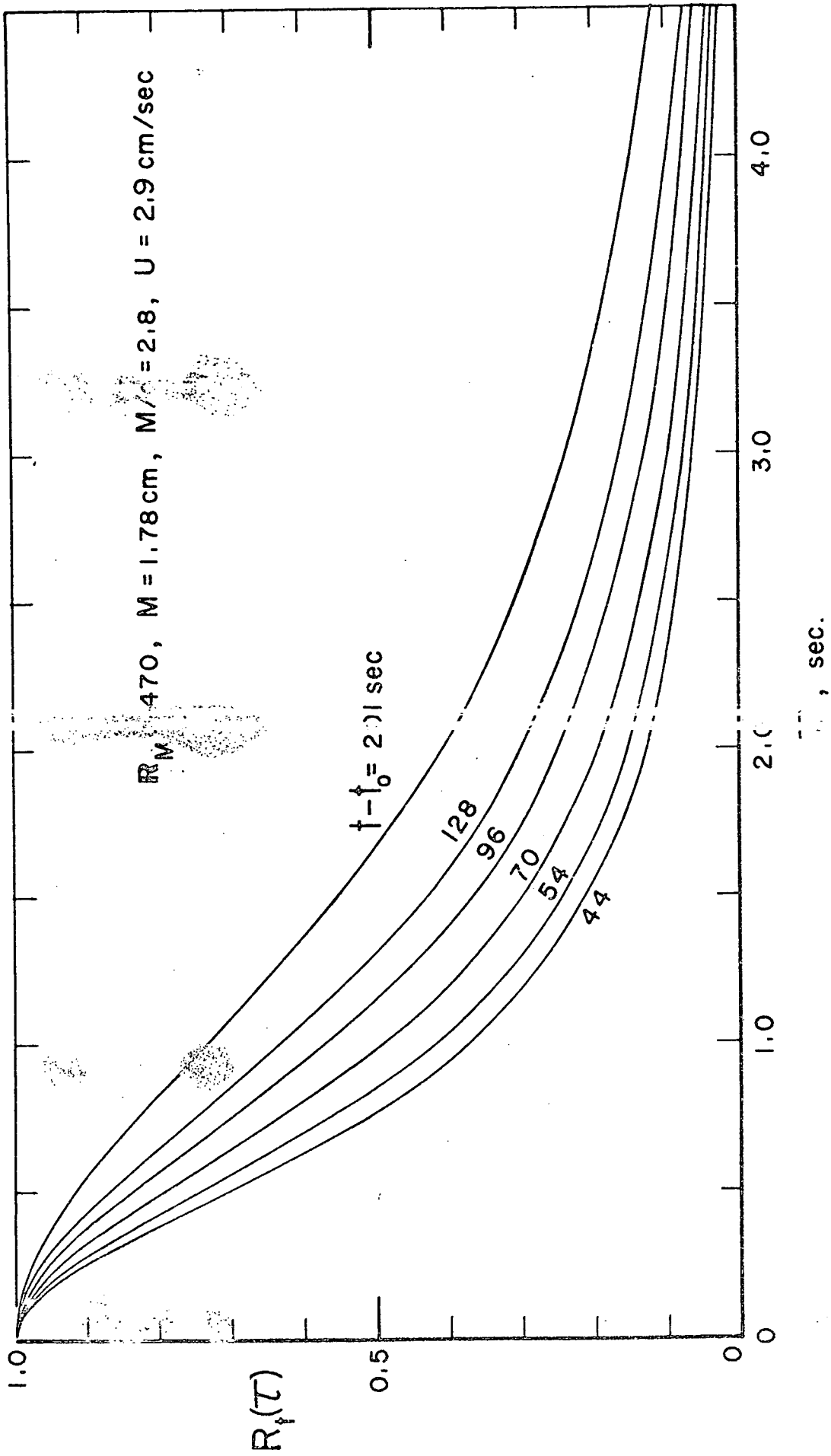
Fig. 8   Time-Correlation Coefficient at Different Stages of Decay (Grid B)
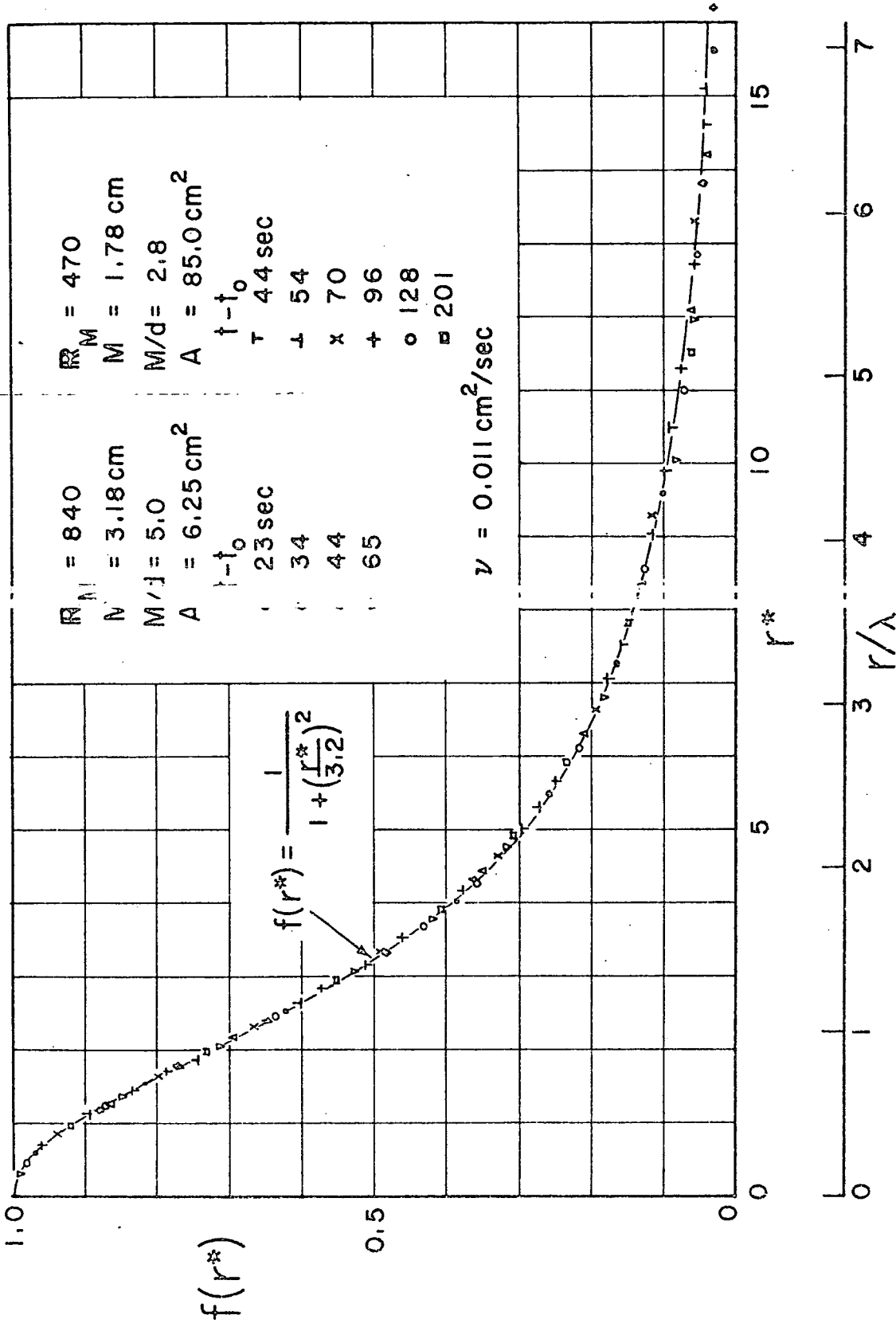
Fig. 9   Measured Self-Preserving Longitudinal Correlation Coefficient of Weak Turbulence
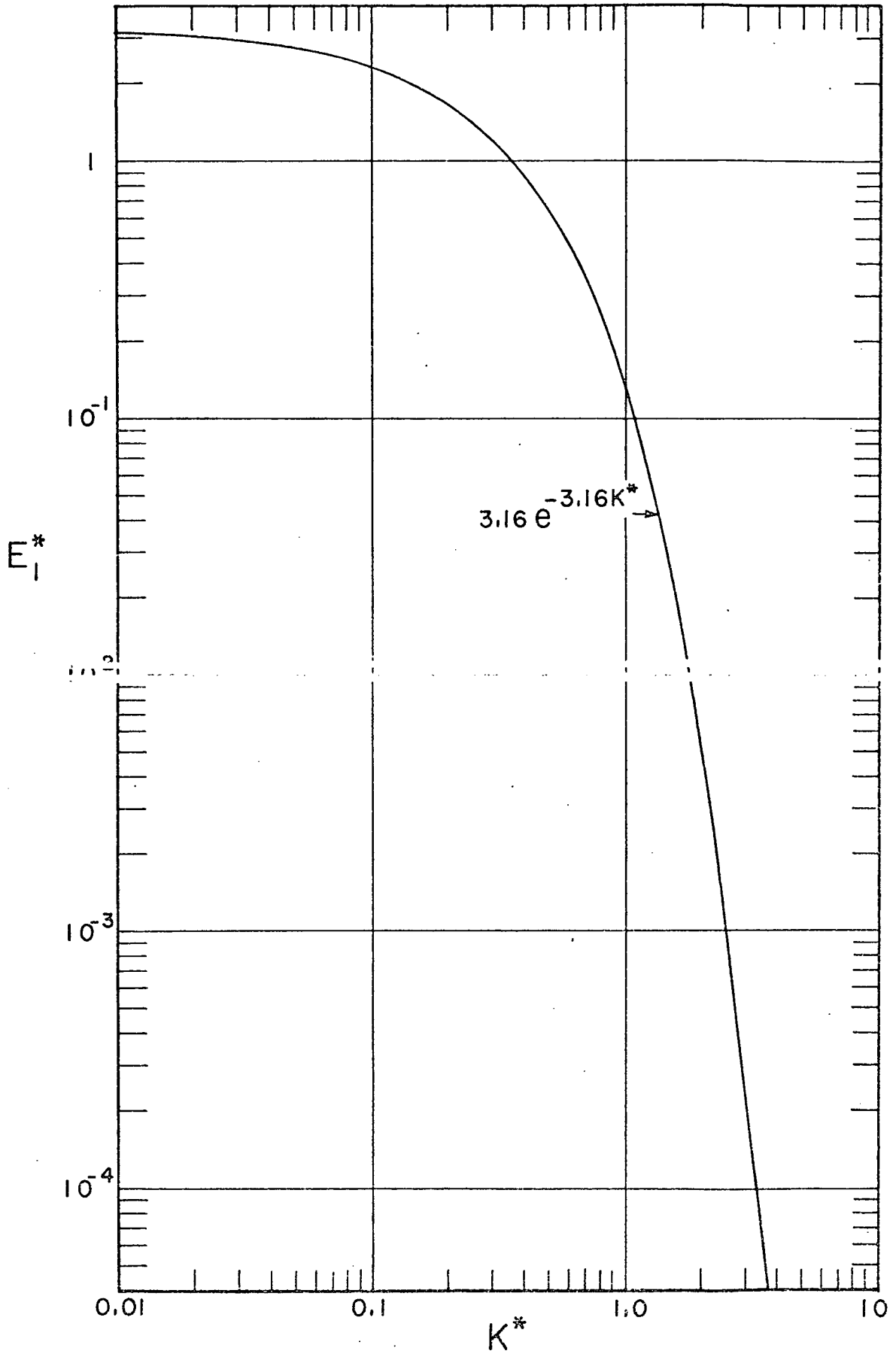
Fig. 10   Dimensionless One-Dimensional Energy Spectrum of Weak Turbulence
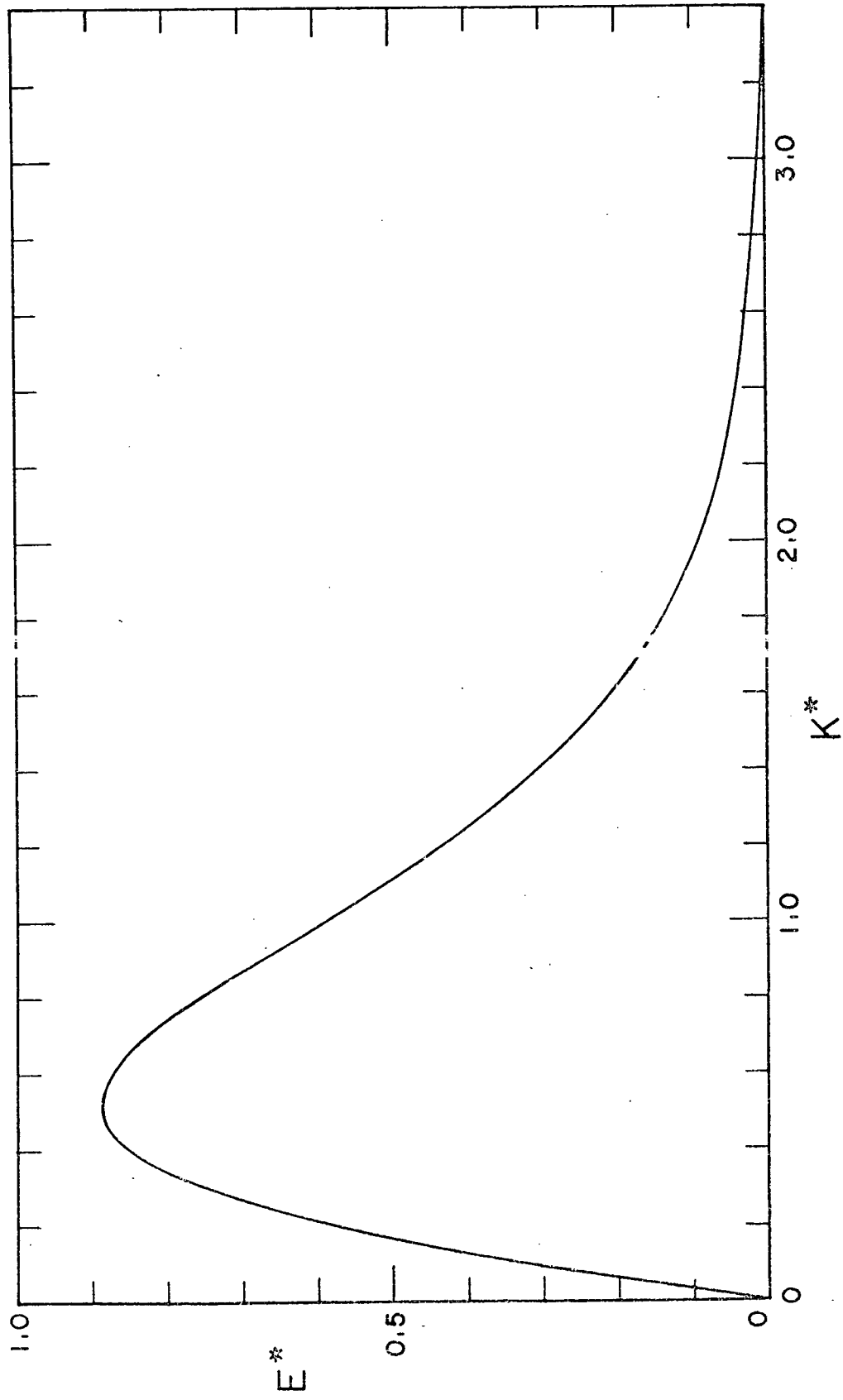
Fig. 11   Dimensionless Three-Dimensional Energy Spectrum of Weak Turbulence
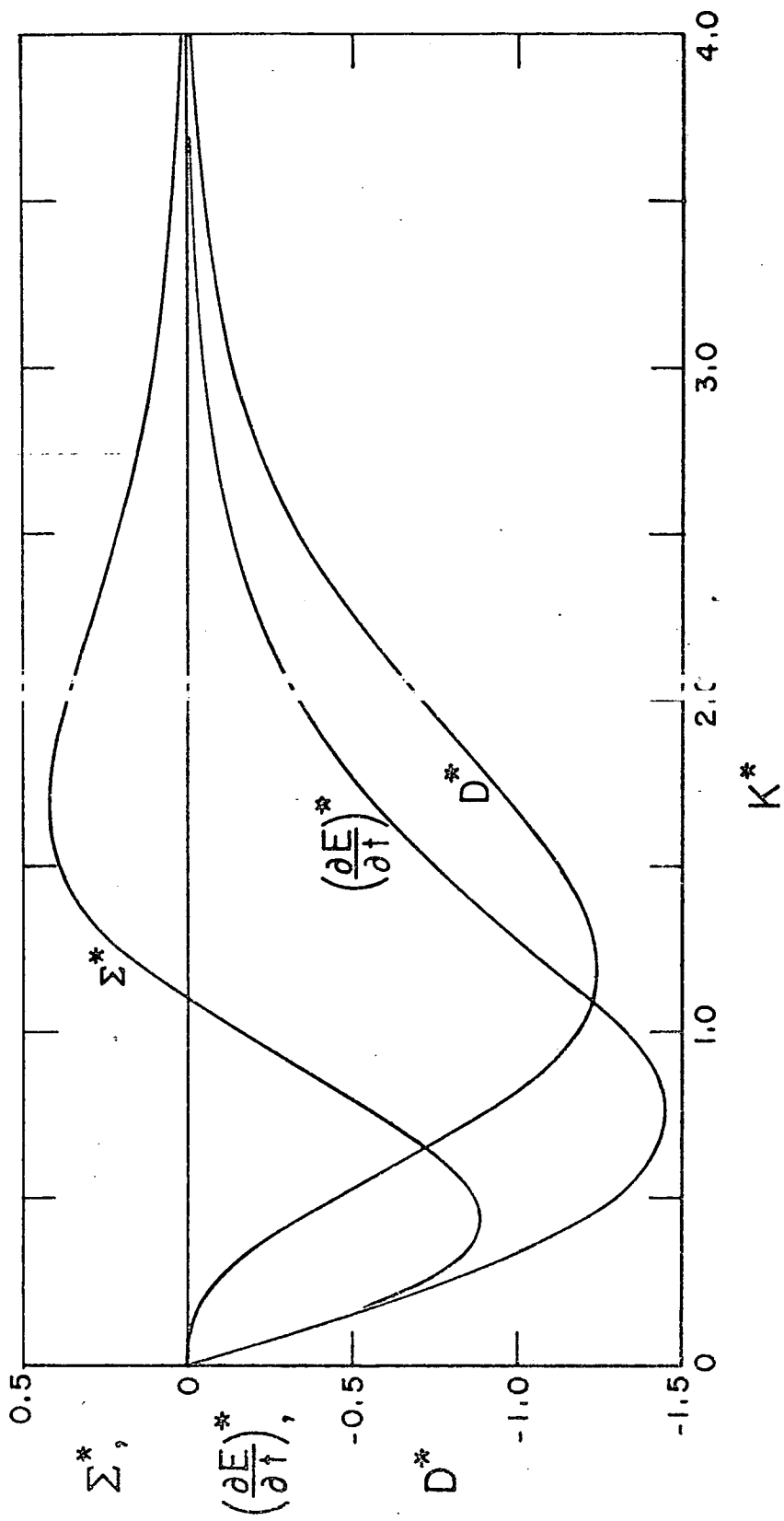
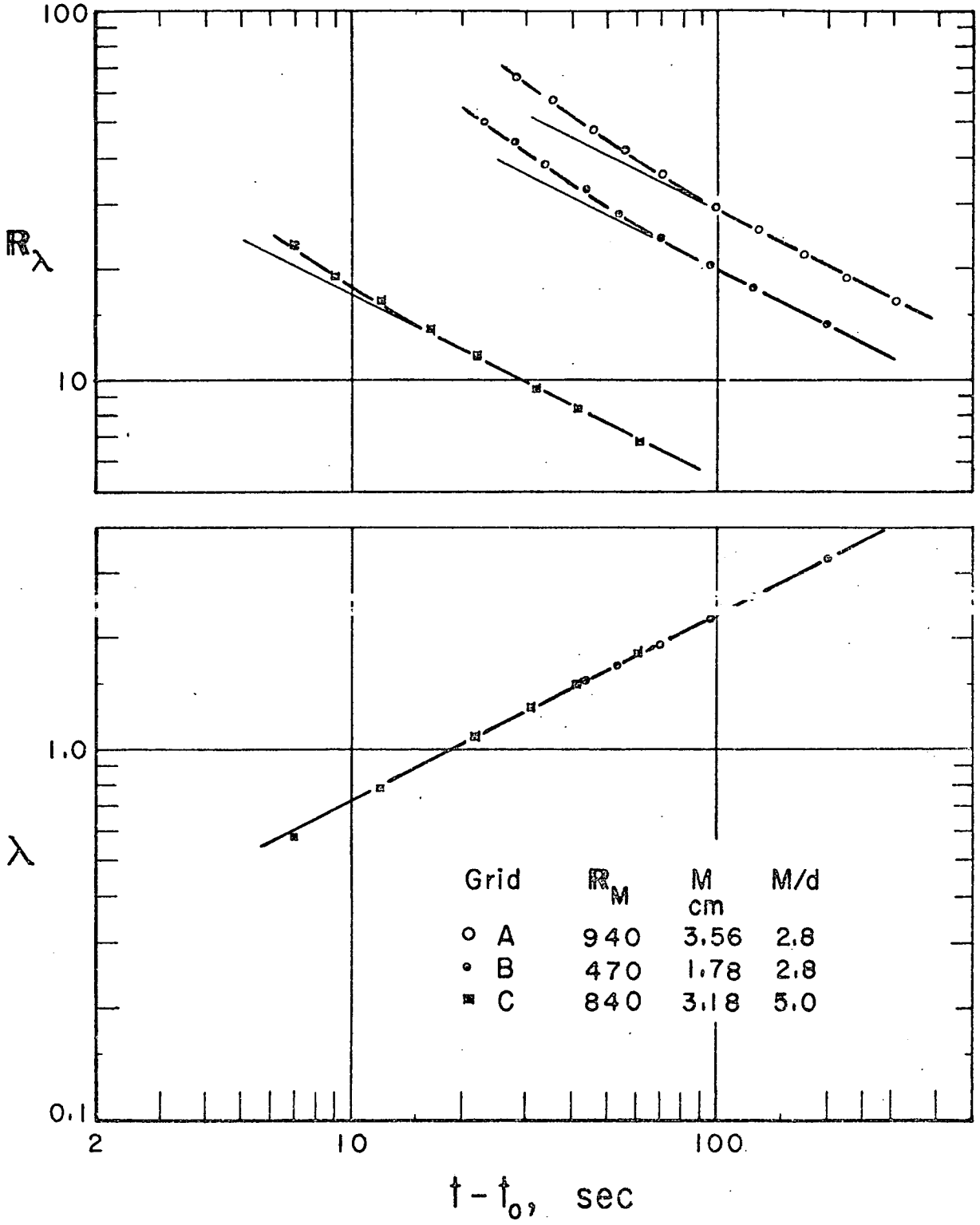Fig. 12   Dimensionless Dissipation Spectrum and Energy Transfer Function of Weak Turbulence

Fig. 13   Reynolds Number of Turbulence and Dissipation Length Parameter
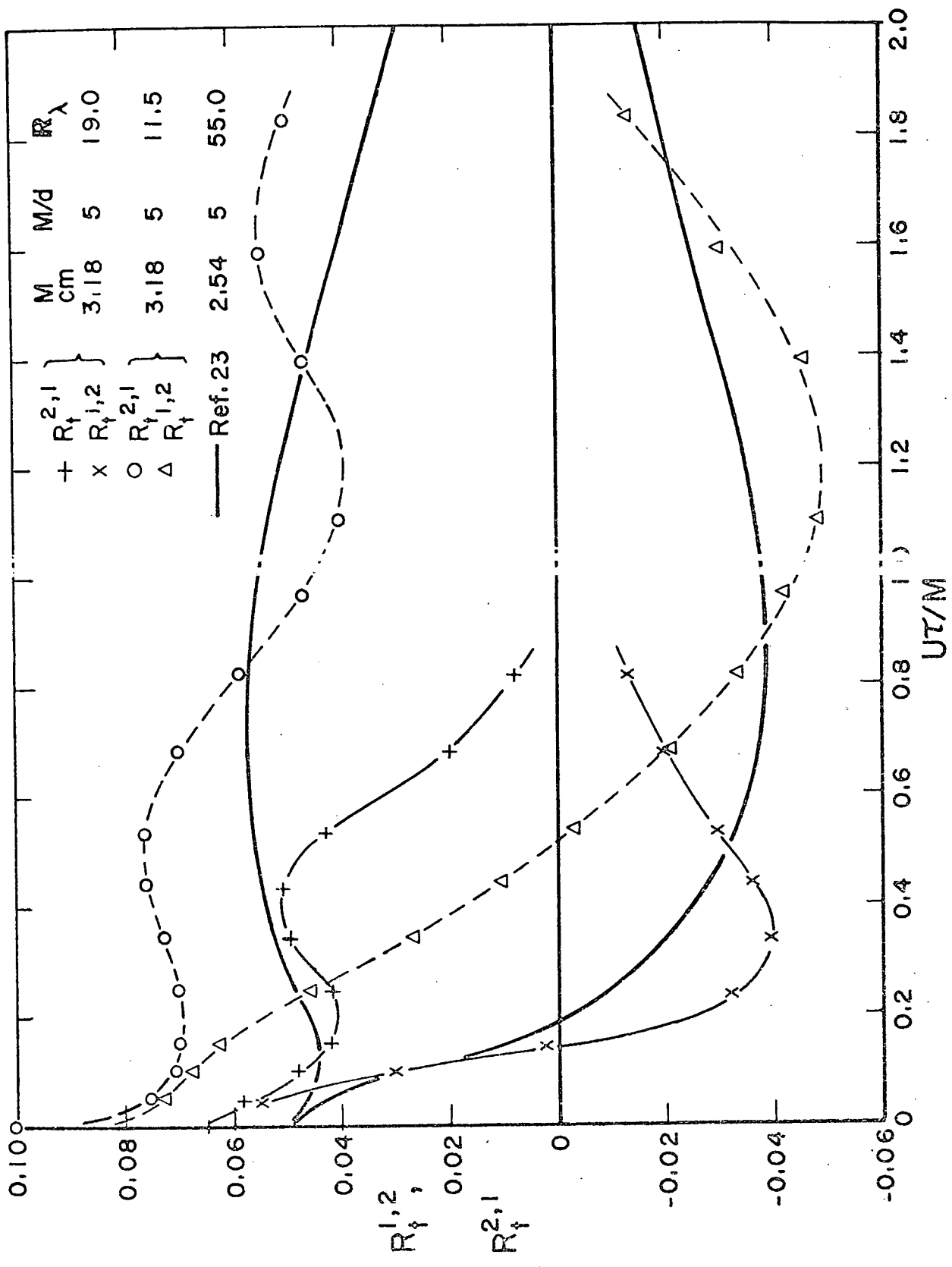as Functions of Decay Time.

Fig. 14   Measured Third-Order Correlation Compared with Data of Frenkiel and Klebanoff (Ref. 23).
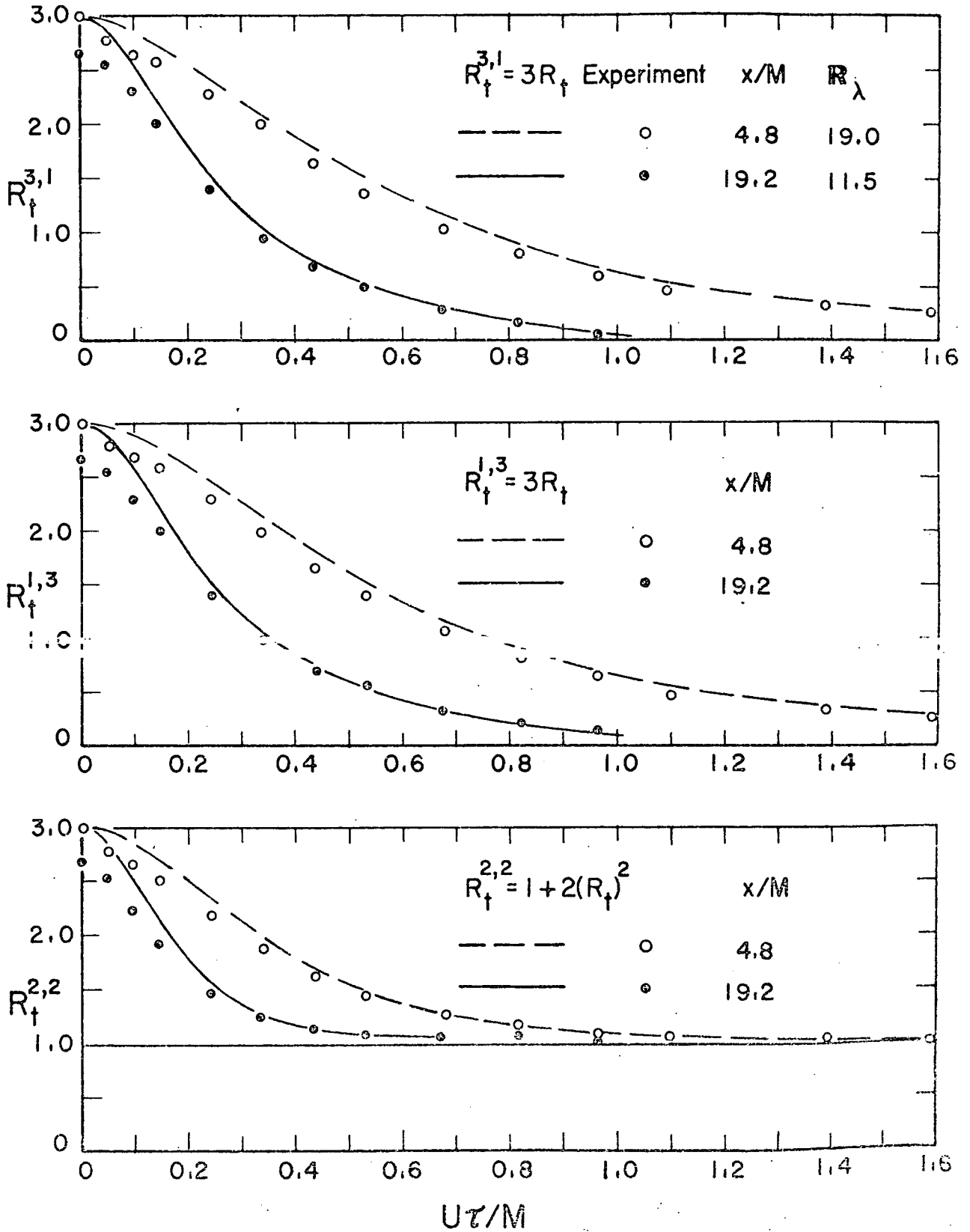
Fig. 15   Measured Fourth-Order Correlation Compared with the Assumption
of Gaussian Probability Density Distribution of Turbulent Velocity